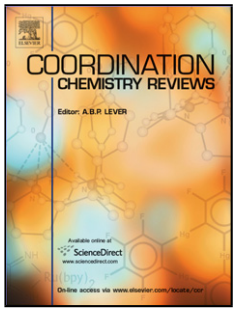

Title: Lanthanide-organic frameworks for gas storage and as magneto-luminescent materials

Author: Syamantak Roy Anindita Chakraborty Tapas Kumar Maji

PII: S0010-8545(14)00092-7
DOI: http://dx.doi.org/doi:10.1016/j.ccr.2014.03.035
Reference: CCR 111856

To appear in: *Coordination Chemistry Reviews*

Received date: 4-11-2013
Revised date: 28-3-2014
Accepted date: 28-3-2014

Please cite this article as: S. Roy, A. Chakraborty, T.K. Maji, Lanthanide-organic frameworks for gas storage and as magneto-luminescent materials, *Coordination Chemistry Reviews* (2014), http://dx.doi.org/10.1016/j.ccr.2014.03.035

Lanthanide-organic frameworks for gas storage and as magneto-luminescent materials

Syamantak Roy[#a], Anindita Chakraborty[#a], and Tapas Kumar Maji[*a]

[a]*Molecular Materials Laboratory, Chemistry and Physics of Materials Unit, Jawaharlal Nehru Centre for Advanced Scientific Research, Jakkur, Bangalore – 560 064, India.*

**E-mail: tmaji@jncasr.ac.in, Phone: +91 80 2208 2826, FAX: +91 80 2208 2766*

[#] Authors contributed equally

ABSTRACT

Smart and careful design strategies need to be adopted for the synthesis of lanthanide-organic framework materials to strike a balance between the high coordination requirement of lanthanide metal ions and the formation of stable and permanently porous structures. Literature reports have documented successful synthesis of such porous lanthanide frameworks with potential application for gas storage. Lanthanide-organic frameworks have also shown promise in a number of magento-luminescent applications. The diverse emission profiles of the lanthanide ions have resulted in tuning the emission colour to generate white-light as well as sense a host of cations, anions and small molecules alike. The permanent porosity has also been used to apply these frameworks as gas storage and separation materials. The exciting magnetic property of the lanthanide-organic frameworks arises from the high orbital contribution and single-ion anisotropy of the lanthanide ions. This eventually ushers the slow relaxation of magnetization with high energy barrier making such systems potential candidates for future magnetic sensory and memory devices. This review will discuss the porous properties of lanthanide-organic frameworks and the progress in utilizing them in gas storage and sensing properties. Colour tunability, white-light emission and magnetic applications in lanthanide-organic frameworks have also been discussed. In conclusion, an overall summary of the properties of these materials and future outlook will be proposed.

Keywords

Lanthanide-organic frameworks, Porous properties, Gas Storage, Luminescence, Magnetism

1. Introduction

The fascinating growth of lanthanide coordination chemistry and supramolecular chemistry during the last two decades have stemmed from the practical successes in catalysis [1,2], biomedical analysis [3], diagnostic and possibly therapeutic medicine [4]. The intrinsic Lewis acidity, magnetic and luminescent properties of these lanthanides (Ln) ions are often not matched by the transition metal ions; thus synthesis of lanthanide based novel functional materials is useful for different applications. The optical properties in lanthanide complexes are particularly interesting, which arise mainly from the 4f-4f electronic transitions [5] and are well studied. But these have weak emission intensities and low quantum yields as they are Laporte forbidden transitions. However, in coordination compounds based on suitable π-conjugated ligands, an energy transfer process occurs from the ligand excited state to the metal excited state and subsequent enhanced emission intensities from the metal centre is realized. This phenomenon is known as 'antenna effect' [6-10]. These types of complexes therefore can overcome the "optical handicap" and show enhanced optical properties. In general, lanthanide ions (Eu^{III}, Pr^{III}, Sm^{III}), (Tb^{III}, Er^{III}) and (Tm^{III}, Ce^{III}) exhibit red, green and blue emission, respectively and by adjusting the relative amounts of these metal ions in a material, multiple colours including white light emitting materials can be accomplished [11-14]. The other significant property of lanthanide-based compounds is magnetism, which has attracted enormous research interest despite its complexity. The magnetic signatures are often difficult to interpret because of the high orbital contribution of the Ln ions and the associated anisotropy. The single-ion anisotropy of Ln ions ushers exciting features like slow relaxation of magnetization which makes the lanthanide-based compounds promising candidates for molecule based magnetic materials. The Ln ions exist almost exclusively in their trivalent state in a coordination complex. The nature of the coordination sphere with variable coordination numbers ($6 \leq CN \geq 13$) is controlled by a subtle interplay between electrostatic interactions and inter-ligand steric constraints. Such versatile coordination geometry of the lanthanide complexes has led to limited success in the design of extended predetermined structures of different dimensionalities. However, by adopting an appropriate synthetic methodology, it is feasible to fabricate stable lanthanide based frameworks with novel functions. These compounds can then be cultivated for a host of magneto-luminescent applications.

Furthermore in recent years, porous coordination polymers (PCPs) or metal-organic frameworks (MOFs) using transition metal ions have developed into a significant area of

research because of its potential applications in gas storage (like H_2, CH_4, and CO_2) [15-18], catalysis [19-21], separations [22, 23], luminescence [24] and drug delivery [25, 26]. For a lanthanide-organic framework (LOF), the gratification of higher coordination number in lanthanides are frequently fulfilled by the coordinating solvent molecules and thus the desolvated framework with unsaturated Lewis acidic Ln^{III} sites can be exploited for specific catalytic activities and interesting adsorption properties like selective adsorption of gases [57]. But the design and synthesis of porous LOFs were less explored compared to the transition metal based frameworks. This is probably due to the difficulty in controlling and predicting the overall structure as the large coordination sphere of lanthanide needs to be filled by multiple linkers that would result in a highly stable condensed structure rather than a porous structure. However, by employing judicious ligand design strategies, it is possible to furnish novel porous LOFs, which can be attractive candidates to study gas storage, sensing of small molecules and guest dependent magnetic and luminescent properties (Scheme 1).

This review will be highlighting mainly the reported extended structures *i.e* coordination polymers of lanthanide based metal ions with different organic linkers. Focus will be on their synthetic approaches, porous, luminescent and magnetic properties. We would then conclude by giving a broad summary and a future perspective of this fascinating material which can be further exploited in different fields of materials science and technology.

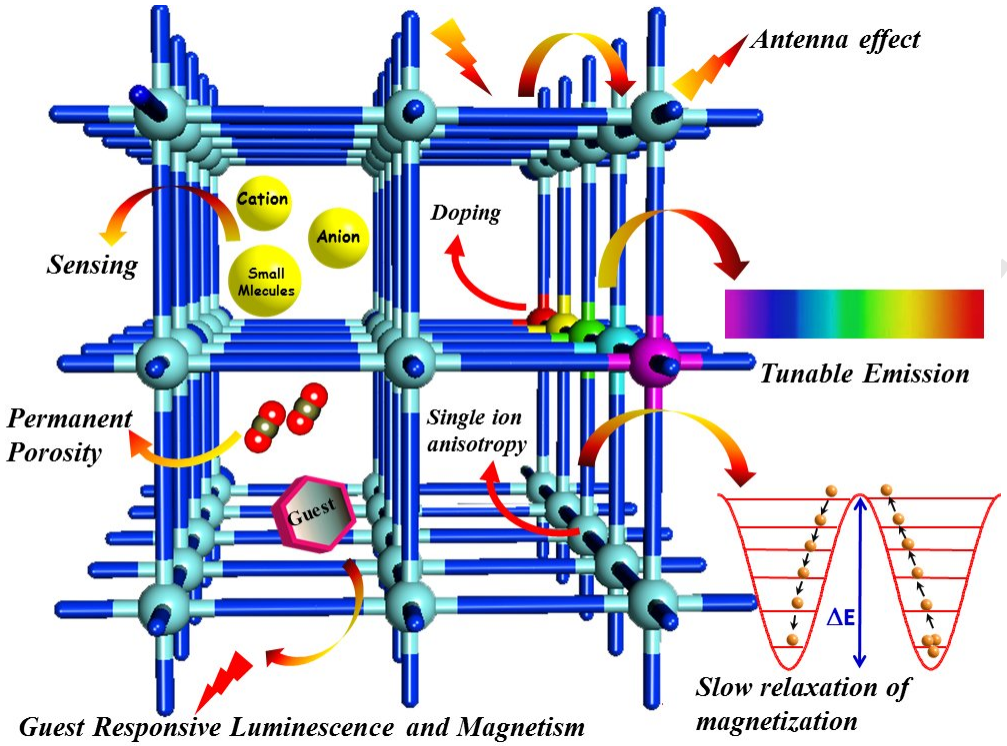

Scheme 1: Schematic representation of porous lanthanide-organic frameworks with versatile functionalities.

2. Synthesis and Design Strategy for the Construction of Higher Dimensional Lanthanide-Organic Frameworks (LOFs)

Synthetic recipes for lanthanide based frameworks have been less discussed compared to the *d*-block elements despite the fact that LOFs are much more interesting in regard to their versatile coordination geometries and the tunable emission, magnetic and porous properties. The scantiness in literature probably stems from the fact that the coordination spheres as well as the structure of lanthanides based frameworks are quite difficult to control and straightforward recipes to synthesize such systems are yet to be developed. It should be noted that although such systems are quite complicated to predict beforehand, the higher coordination number can result in unanticipated and remarkable unprecedented structural topology. In addition to such structural novelty, these compounds can also render high thermal stability which is not easily achievable in other cases (transition metal based framework). The high coordination number of the metal ions is advantageous in another way too. Solvent molecules often coordinate to the metal to fulfil the coordination sphere and in such instances, removal of coordinated solvents can result in the generation of UMSs, which

are very much intended for H_2 storage and CO_2 capture applications [27]. Such framework with Lewis acidic sites showed potential catalytic activities in different organic reactions [2].

Therefore to furnish such functional lanthanide framework, a judicious synthetic strategy is necessary owing to the complexity of lanthanide systems. Ln-organic frameworks have been mostly synthesized by combining organic ligands and metal salts in solvothermal reactions. Room temperature solvent evaporation and solvent diffusion have also been employed to furnish such compounds. The choice of ligand system is very crucial. Since the lanthanide ions are inherently hard centres, hard donor sites are required for the fabrication of lanthanide framework. Use of carboxylate based ligands like succinate, mucicate, oxalate have widely been used. Larger linkers like 1,4-benzene dicarboxylate (BDC) [28], thiophene-2,5-dicarboxylate [29], 4,4'-dicarboxylate-2,2'-dipyridine (BPDC) [30] have also been exploited. The use of such linkers led to different new framework structures of different dimensionalities based on the versatile binding modes of the carboxylate groups. The Ln ions in such diverse structures can locate themselves in different connected nodes, such as four [30], six [31], seven and eight connected nodes [32]. Several interesting structures and unusual topologies of lanthanides have been reported, but synthesis of such LOFs with appropriate ligand design strategy need to be explored properly. Detail discussions in this regard are beyond the scope of the current review. It is clear that lanthanide-organic frameworks have huge potentials for furnishing novel structures and new synthetic routes should open up new directions for fabricating such structures.

3. Porous Lanthanide-organic Frameworks: Permanent Porosities and Gas Storage /Separation Applications

The capture and storage of CO_2 and H_2 gas molecules are of primary environmental importance for atmospheric clean-up and clean energy applications. There has been an alarming rise in the CO_2 atmospheric levels over the last few decades and this trend is set to continue due to the rapid industrial growth which is happening chiefly in the developing nations [33]. In order to arrest the disturbing rise of CO_2 levels in the atmosphere, research in carbon capture and sequestration (CCS) technologies have gained significant interest. The massive consumption of petroleum is also contributing to the escalating pollution levels by releasing CO_2 gas into the atmosphere. The development of a “cleaner” substitute for gasoline is therefore a hot-topic of research and H_2 gas has been found to be an effective

substituent. The promising nature of H_2 gas as an operational "clean" fuel is because of its high specific energy, carbon-free nature and a high abundance [34]. But the hurdle that needs to be overcome is its difficulty in storage and transport over long distances. It has to be compressed at high pressures or stored cryogenically for storage and transport which increases the cost of its practical use and also the weight of the storage material which becomes cumbersome over a long distance. The focus therefore shifts to the development of light-weight and low-cost materials which can reversibly take up and release H_2 at ambient temperatures and pressures.

Porous materials such as zeolites and metal-organic frameworks (MOFs based on *d*-block metal ions) which have shown the potential for adsorption of CO_2 and H_2 [16-18, 35-39]. MOFs are found to be the most promising materials due to their permanent and uniform porosity, high surface area, structural diversity, a variety of topologies and ease of pore modification. Exceptional uptake of H_2 and CO_2 in lanthanide-organic frameworks however is rare but these rare-earth based porous materials have been proven to be ideal systems for the study of the mechanism and nature of physisorption. So far several reviews regarding the gas storage properties of MOFs have appeared but a systematic library of lanthanide-organic frameworks used for gas storage properties have yet to be documented.

3.1. *Porous properties*

Lanthanide metal ions have been known to have large coordination numbers which are in the range of 6-13. It is this property that makes the synthesis of stable and permanently porous framework structures with lanthanide ions very difficult. In most lanthanide coordination environments, ancillary ligands like water or other solvent molecules like DMF "make up" the vacant coordination sites, but in general their removal results in the collapse of the framework structure. Kiritsis *et al.* reported the synthesis of a La^{III} based porous 3D coordination polymer $\{[La_2(ad)_3(H_2O)_4].6H_2O\}_n$ (ad = adipato; $C_6H_8O_4^{2-}$) which reversibly transformed into a non-porous structure upon water removal $[La_2(ad)_3(H_2O)_2]_n$ [40]. Although the framework was stable upon water removal, porosity was lost due to structural transformation upon dehydration and the original structure was recovered when stirred overnight in a water medium. The PXRD data further proved the reversible structural interconversion. The synthesis of stable and permanently porous LOFs therefore remained a huge challenge until Yaghi *et al*. synthesized an extended Tb-organic framework $\{Tb_2(bdc)_3{\cdot}(H_2O)_4\}_n$ (bdc = 1,4-benzenedicarboxylic acid) which generated permanent

microporosity upon solvent removal [28]. The asymmetric unit showed the presence of a Tb^{III} atom, one and a half bdc and two water molecules. The Tb^{III} centre was octacoordinated by monodentate coordination of six bdc oxygen atoms and two water molecules. The structure could be envisioned as eight Tb^{III} atoms occupying the eight corners of a parallelepiped with bdc at four of its face (*ab* and *bc* planes). Another bdc polymerized the structure into a condensed 3D network (Fig. 1a). The water molecules occupied the *ac* plane and upon removal of these water molecules an extended 1D channel opened up along the crystallographic *b* axis (Fig. 1b). Thermogravimetric analysis (TGA) showed that the dehydrated and microporous framework $\{Tb_2(bdc)_3\}_n$ was generated at 115˚C. PXRD pattern of the dehydrated framework showed similarity to that of the as-synthesized framework suggesting the same structural topology. The microporous framework was then stable up to 450˚C. This study was important in showing the approach of converting a condensed non-porous structure into a stable and porous framework structure.

In a similar kind of investigation, Yaghi *et al.* synthesized a stable and permanently microporous terbium organic framework $\{Tb(bdc)(NO_3)\cdot 2DMF\}_n$ which was stable even after the removal of the DMF molecules (Fig. 1c) [41]. The PXRD pattern of the desolvated framework showed broad signals indicating a breaking of long range order. However similar sharp peaks as that of the as-synthesized frameworks were observed upon exposure to DMF molecules. The single crystal structural analysis showed that each carboxylate group acted as a bridge between two Tb^{III} centres in a bis-monodentate fashion and generated chains along the crystallographic *c*-axis (Fig. 1d). The chains were further cross-linked by BDC to generate a 3D structure where the nitrate anions and DMF pointed into the channels (Fig. 1c). The desolvated framework $\{Tb(bdc)(NO_3)\}_n$ showed thermal stability up to 320˚C. CO_2 uptake at 195 K revealed a typical type-I curve and indicated the presence of permanent porosity in the desolvated framework (Fig. 1e). Also, the removal of guest molecules left open metal sites within the framework for potential use as sensors and other applications. Ferey *et al.* were also successful in synthesizing porous and highly stable LOF $Eu_3(H_2O)(OH)_6[C_6H_3(CO_2)_3]\cdot 3H_2O$ (MIL-63) and $Eu_2(O_2C\text{-}C_{10}H_{14}\text{-}CO_2)_3$ [MIL-83(Eu)]. MIL-63 showed the presence of both inorganic 2D net and zeolitic behaviour and was the first report of a thoroughly characterized porous Eu-carboxylate framework [42,43].

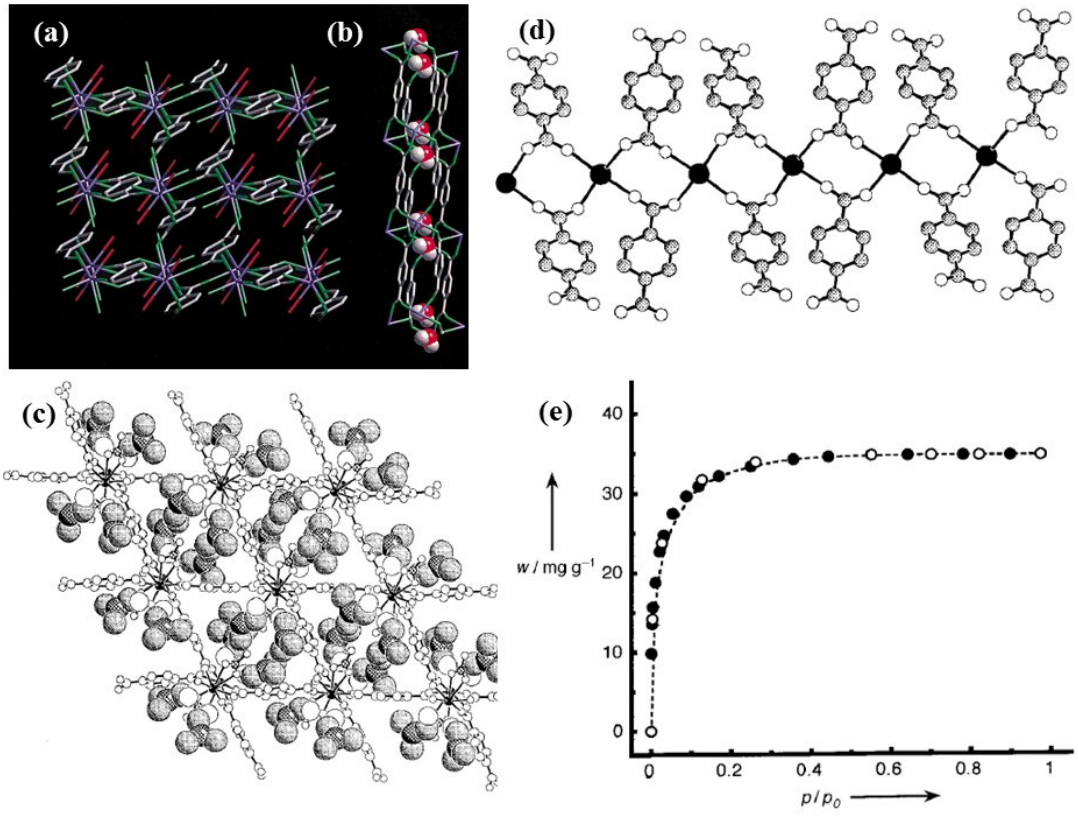

Fig. 1. (a) The crystal structure of $\{Tb_2(bdc)_3 \cdot (H_2O)_4\}_n$ shown approximately along the crystallographic *b*-axis (Tb, blue; C, gray; O (carboxylate), green; and O (water), red). (b) Water distribution along the channels emphasized by a view along the crystallographic *a*-axis. (c) Structure of $\{Tb(bdc)(NO_3) \cdot 2DMF\}_n$ in a projection along the *c*-axis with DMF shown in space filling (C, shaded; N,cross-hatched; O, open) and the Tb-bdc-NO_3 framework as ball-and stick (Tb, filled; N, cross-hatched; C and O, open) (d) representationsView of Tb-bdc chains perpendicular to the *c*-axis. (e) CO_2 adsorption isotherm (sorption (dark circles) and desorption (open circles)) for $\{Tb(bdc)(NO_3)\}_n$. Reproduced with permission from Ref. [28,41]

Schröder *et al.* synthesized two isostructural three dimensional porous LOFs $[Ln_2(PDC)_3(DMF)_2]_n$ (PDC = pyridine-3,5-dicarboxylate; Ln = Er^{III} or Y^{III}) [44]. Thermogravimetric analysis of the two lanthanide frameworks showed that all the free solvent molecules and the coordinated DMF molecules were lost below 200˚C and the desolvated framework was further stable up to 470˚C retaining its structural integrity and crystallinity. The desolvated framework was generated upon heating and structural transformation was realized. The transformation involved a rearrangement of the framework core with the loss of both coordinated and guest solvent molecules. Such crystal to crystal

transformation in lanthanide systems was documented for the first time in this report. The desolvated frameworks showed a typical type-I N_2 adsorption profile suggesting microporous nature of the framework. Benzene adsorption isotherms were also of similar nature. The work was important in giving conclusive proof of the structural transformation through crystallographic data.

A series of porous and thermally stable isomorphous lanthanide-organic frameworks $\{Ln(BTC)(H_2O)\cdot(DMF)_{1.1}\}_n$ (BTC = 1,3,5-benzenetricarboxylate; Ln = Y, Tb, Dy, Er, Yb), were reported by Xu *et al*. which were stable above 450˚C [45]. At a temperature range of 315°C to 345°C, the frameworks lost the guest and coordinated solvent molecules to generate the $\{Ln(BTC)\}_n$ frameworks. The intactness of the crystallinity of the desolvated frameworks were validated by the PXRD patterns which showed similarity with the patterns of the as-synthesized framework. N_2 adsorption measurements at 77 K and 1 atm pressure revealed microporous nature of all the frameworks. This was the first report of carboxylate based frameworks with both high porosity and excellent thermal stability to be utilized in gas storage, catalysis and other applications.

It is therefore clear that in spite of the challenges and difficulties facing the construction of permanently porous and stable lanthanide frameworks, a lot of progress has been made for the synthesis of permanent porous and stable frameworks [46-53]. These frameworks can be and are being utilized for a host of applications such as gas storage, separation, mechanistic studies, catalysis, sensing, colour tunability etc.

3.2. *H_2 storage*, *CO_2 capture and separation using porous lanthanide frameworks*

In 2008, Zhou *et al.* published very important results where they have explained that an optimal pore size contributes to a greater interaction between the pore walls and H_2 molecules thus giving rise to an increased uptake [54]. They synthesized a Y^{III} based lanthanide-organic framework $\{Y(BTC)(H_2O)\cdot 4.3H_2O\}_n$, which showed a 1.57 wt% uptake of H_2 at 77 K and 1 atm pressure. The crystal structure revealed that the BTC ligands bridge the Y^{III} to form a tetragonal porous framework with channels along the crystallographic *c*-axis of dimensions 5.8 × 5.8 $Å^2$ (Fig. 2a). The framework also showed selectivity of H_2 over N_2 and isosteric heat of H_2 adsorption was found to be 7.3 kJ/ mole. At 77 K and 10 bar pressure, the H_2 uptake was found to be 2.1 wt% (Fig. 2b). The researchers performed powder neutron diffraction study on this framework with D_2. The study revealed that an optimal pore size which is slightly greater than double the kinetic diameter of H_2 (~6 – 7 Å)

enhances the interaction of the H_2 molecules with the pore walls thereby increasing the uptake amount. The authors proposed that the optimal size promotes increased van der Waals interaction between the gas and the pore walls and competes with the interaction of H_2 with the open Y^{III} sites present within the system (Fig. 2c). This study for the first time gave direct structural information about the interaction of H_2 molecules with the pore walls resulting in higher uptake and this will be useful for future design of lanthanide-organic frameworks apt for high H_2 uptake capacity.

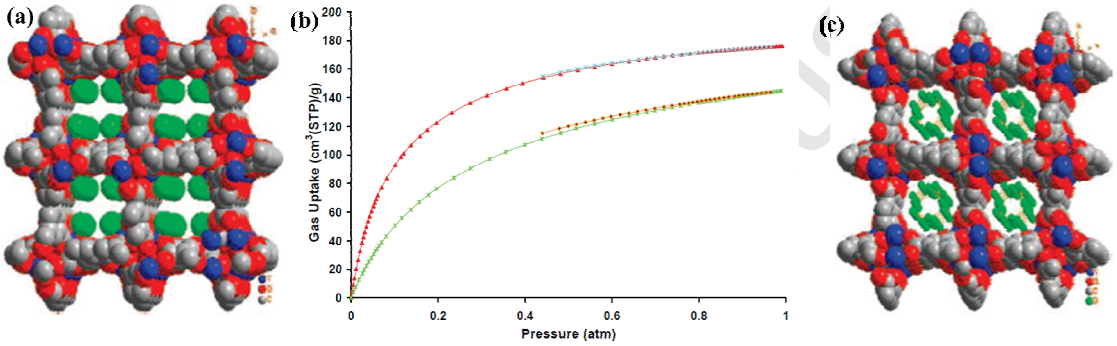

Fig. 2. (a) Structure of the porous $\{Y(BTC)(H_2O)\cdot 4.3H_2O\}_n$ shown containing coordinated water molecules (green) inside the pores . (b) H_2 adsorption isotherms at 77 K (red/light blue), and at 87 K (green/orange).and (c) Structural characterization of hydrogen clusters formed inside the framework of $\{Y(BTC)(H_2O)\}$. Reproduced with permission from Ref. [54]

Recently we have reported a porous bimetallic alkali (K^I)-lanthanide Ho^{III} framework based on an oxalate ($C_2O_4^{2-}$) linker [27]. The structure $\{KHo(C_2O_4)(H_2O)_4\}_n$ has several interesting characteristics. Here each octacordinated Ho^{III} centre is chelated to four different $C_2O_4^{2-}$ linkers and the resulting $Ho(ox)_4^{5-}$ linked to another four Ho^{III} and four eight coordinated K^I centre resulting in a 3D framework. Each octacoordinated K^I is ligated to four μ_2-O atoms from ox^{2-} which acts as a tetradentate bridging ligand (Fig. 3a) and four water molecules. The framework has bidirectional channels, like 1D square shaped channels (3.6×3.6 $Å^2$) along *c*-axis which is occupied by the four K^I-bound water molecules. The dehydrated framework also showed small channels perpendicular to *a*-axis with pore dimensions of 2×1.2 $Å^2$ (Fig. 3 b, c). This is one of the rare compounds synthesized so far where the eight coordination sites of Ho^{III} are satisfied by the oxalate linker, no additional solvent molecules are attached to satisfy the higher coordination number of the lanthanide

ion, which acts as a negative point. Secondly, K^I ions are periodically placed in the framework and the dehydrated framework with such unsaturated sites is an ideal platform to study the gas storage properties particularly H_2 and CO_2.

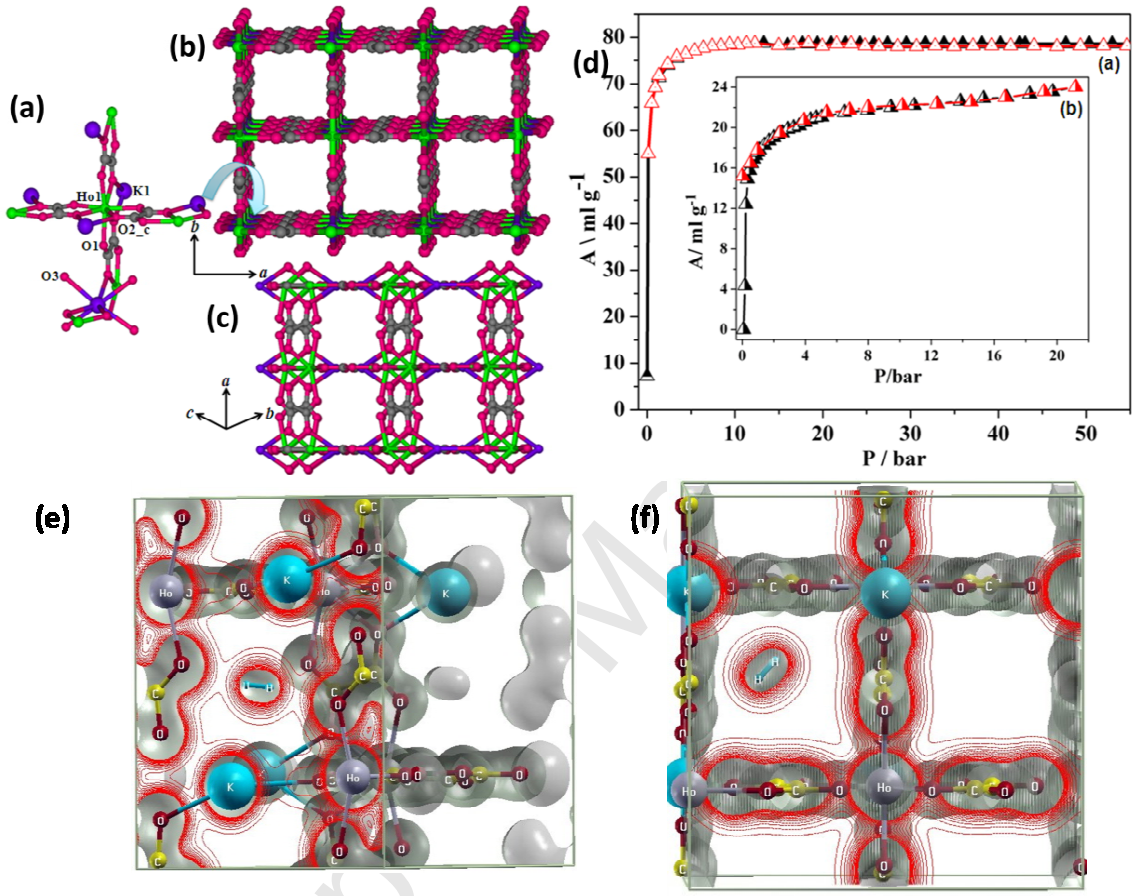

Fig. 3. (a) Coordination environment of Ho^{III} and K^I shown in $\{KHo(C_2O_4)_2(H_2O)_4\}_n$. (b) Square shaped channels along the crystallographic *c*-axis shown for the 3D framework. (c) View along parallel direction to *a*-axis showing small channels of the 3D framework. K-bound water molecules were removed. (d) High-pressure H_2 and CO_2 sorption isotherms for the dehydrated framework. (a) H_2 at 77 K; (b) CO_2 at 298 K (inset)**.** Figures of Iso-surfaces of charge density (iso-value=0.5 a.u.) of the optimized structure of an H_2 molecule adsorbed inside a (e) small pore of the framework simulated from first-principles: the molecular axis of H_2 is parallel to the line joining the centre of mass of H_2 with K site and (f) big square pore of the framework simulated from first-principles: the molecular axis of H_2 is perpendicular to the line joining the centre of mass of H_2 with K site. Reproduced with permission from Ref. [27]

The framework shows very high thermal stability (up to 380˚C). The Langmuir surface area of the framework is ~ 325 m^2/g. The isosteric heat of adsorption for CO_2 is about 26.3 kJ/mol. The framework showed 0.7 wt% of H_2 uptake at 77 K under high pressure (Fig.3d). Steep uptake of H_2 at low pressure regions at 77 K and 1 atm has been correlated to the strong interaction of H_2 with the pore surface decorated with unsaturated K^I sites. The strong hydrophilic nature of the pore surface is also realized by typical type I adsorption profile with H_2O. The isosteric heat of adsorption for H_2 at low coverage region is -9.21 kJ/mol obtained from Clausius–Clapeyron equation. This value is significantly high in MOF systems as it generally shows 5-6 kJ/mol. The DFT based first principle calculations suggest that the strongest interaction occurs when H_2 is in the small pore and close to K-site with the configuration of K-site lied on the perpendicular bisector of the H-H bond. In the bigger pore, H_2 atom was observed close to the K^I site and the corresponding ΔH_{ads}= -9.03 kJ/mol value obtained from DFT calculation agrees well with the experimental results (Fig. 3e,f). This is the first report where highly electropositive alkali metal cations are arrested as an essential part of the framework in a periodic manner along the pore surface.

A recent report by Eddaoudi *et al.* revealed the fact that an improved CO_2 adsorption energetics of a material depends on the synergistic effect of open metal sites and a proximal high local charge density present within the structure [55]. The researchers synthesized a series of **fcu** type LOFs and studied the CO_2 and H_2 adsorption and energetics of CO_2 adsorption preliminarily on two such structures $[[(CH_3)_2NH_2]_2[Tb_6(\mu_3\text{-}OH)_8(FTZB)_6(H_2O)_6]\cdot(H_2O)_{22}]_n$ and its Y^{III} analogue $[[(CH_3)_2NH_2]_2[Y_6(\mu_3\text{-}OH)_8(FTZB)_6(H_2O)_6]\cdot(H_2O)_{52}]_n$. The crystal structure of the Tb^{III} framework showed that the Tb^{III} centres is nine coordinated that are satisfied by four μ_3-OH groups, four oxygen/nitrogen atoms of the carboxylate groups and/or tetrazolate rings and the ninth coordination site is satisfied by a water molecule (Fig. 4a).The overall structure is generated as follows: The Tb^{III} ions are bridged in a bis-monodentate fashion by μ_3-OH and the deprotonated carboxylate and/or tetrazolate rings generating the molecular building block (MBB) $[Tb_6(\mu_3\text{-}OH)_8(O_2C^-)_6(N_4C^-)_6]$. Now a 3-periodic framework is formed by the bridging of each of these MBB's by $FTZB^{2-}$ (Fig. 4a). The CO_2 uptake of the Tb^{III} and Y^{III} compounds at 298 K and 760 Torr are 15.6 and 18.1 wt.% respectively. The interesting fact was that at very low pressures (0.01 bar) the CO_2 uptake was the second highest reported so far after Mg-MOF 74 (Fig. 4b). A thorough Q_{st} analysis was done to explain the exceptional CO_2 adsorption characteristics (Fig. 4c). A comparison of the Q_{st} values between $[[(CH_3)_2NH_2]_2[Tb_6(\mu_3\text{-}$

$OH)_8(FTZB)_6(H_2O)_6]\cdot(H_2O)_{22}]_n$, its Y^{III} analogue and the frameworks constructed from an elongated fluorinated linker expectedly show different values. Higher Q_{st} values were calculated from $[[(CH_3)_2NH_2]_2[Tb_6(\mu_3\text{-}OH)_8(FTZB)_6(H_2O)_6]\cdot(H_2O)_{22}]_n$, its Y^{III} analogue where the close proximity between the open metal sites, fluorine atoms and tetrazolate moieties created a high local charge density encouraging synergistic effects. Therefore, the authors proposed that the combined effects of the presence of a high concentration of open metal sites and electronegative hetero F and N atoms within a narrow space and close to the open metal sites contributed to the highly favoured multisites interactions with a single CO_2 molecule giving rise to enhanced CO_2 adsorption. Interestingly, the framework also showed good potential to selectively capture CO_2 over N_2 as realized by breakthrough measurements (Fig. 4d).

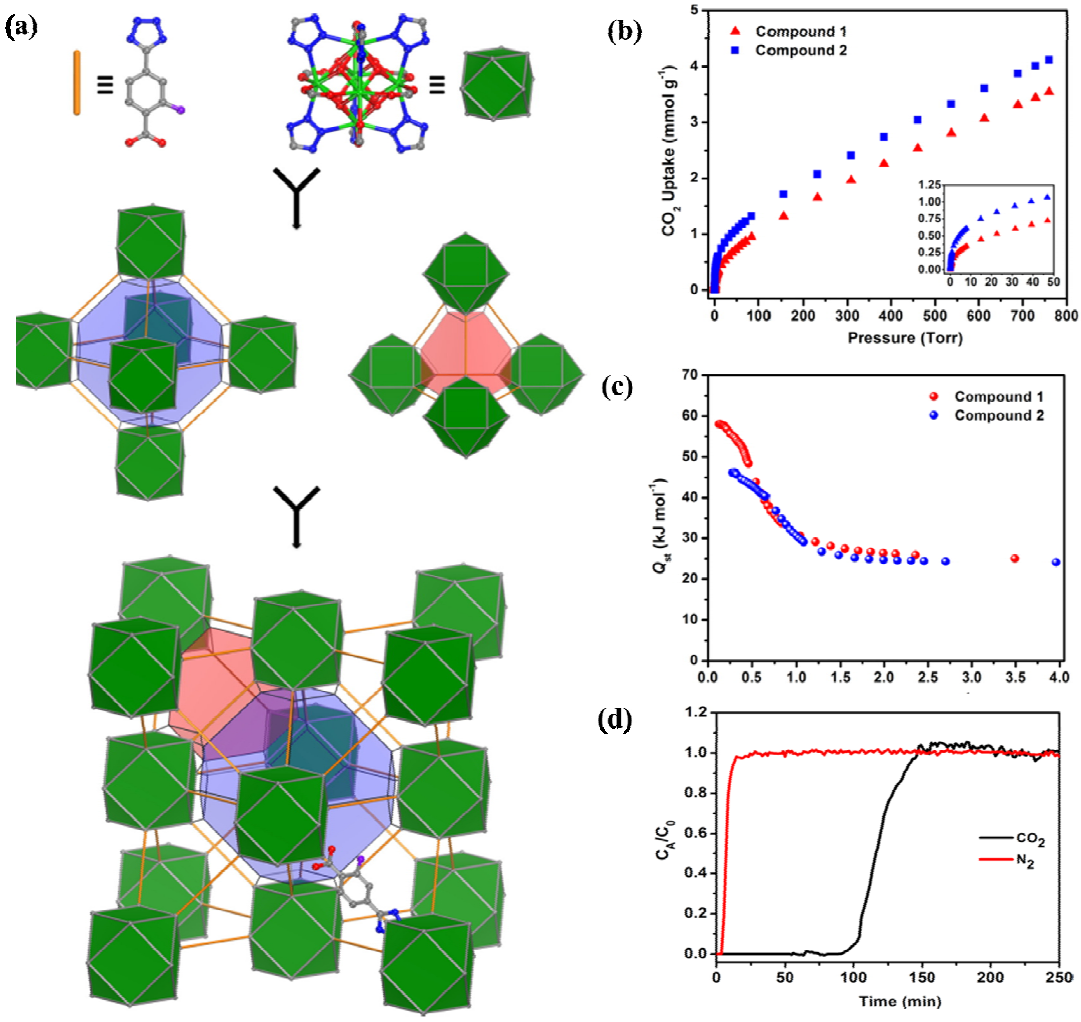

Fig. 4. (a) Structural representation of $[[(CH_3)_2NH_2]_2[Tb_6(\mu_3\text{-}OH)_8(FTZB)_6(H_2O)_6]\cdot(H_2O)_{22}]_n$: organic and inorganic MBBs, $FTZB^{2-}$ and the 12- connected Tb-based cluster respectively which can be viewed as a linear connection and cuboctahedron node to afford the augmented fcu net, consisting of octahedral and tetrahedral cages shown as blue and pink truncated polyhedron, respectively are shown from top to bottom, Hydrogen atoms and coordinated water molecules are omitted for clarity. (Tb = green, C = grey, N = blue, O = red, F = purple) (b) CO_2 adsorption isotherms for $[[(CH_3)_2NH_2]_2[Tb_6(\mu_3\text{-}OH)_{8(}FTZB)_6(H_2O)_6]\cdot(H_2O)_{22}]_n$ and $[[(CH_3)_2NH_2]_2[Y_6(\mu_3\text{-}OH)_8(FTZB)_6(H_2O)_6]\cdot(H_2O)_{52}]_n$ at 298 K. The inset shows the steep uptake at low pressure up to 50 Torr. (c) Plot of Q_{st} value calculations from the 258, 273, and 298 K adsorption isotherms in $[[(CH_3)_2NH_2]_2[Tb_6(\mu_3\text{-}OH)_{8(}FTZB)_6(H_2O)_6]\cdot(H_2O)_{22}]_n$ and $[[(CH_3)_2NH_2]_2[Y_6(\mu_3\text{-}OH)_8(FTZB)_6(H_2O)_6]\cdot(H_2O)_{52}]_n$ (d) Experimental breakthrough experiment of CO_2/N_2 mixtures on **[**$[(CH_3)_2NH_2]_2[Tb_6(\mu3\text{-}OH)_{8(}FTZB)_6(H_2O)_6]\cdot(H_2O)_{22}]_n$. Reproduced with permission from Ref. [55]

Selective gas adsorption has been applied as a useful technique in the industry for purification and isolation purposes. Adsorptive separation relied upon on a number of mechanisms such as molecular sieving effect, thermodynamic equilibrium effect, kinetic effect or the quantum sieving effect [56]. MOFs containing permanent porosity, tunable pore size and facile pore surface functionalization have therefore been utilized to a significant extent. Lanthanide based frameworks with no exception from other classes of MOFs show the same potential for adsorptive separation of gas molecules.

The first report of porous lanthanide organic framework for selective gas adsorption was published by Kaneko *et al*. in the year 2003 [57]. The structure of the $[\{Er_2(PDA)_3(H_2O)\}\cdot 2H_2O]_n$ (PDA = 1,4-phenylendiacetate) showed the presence of two crystallographically independent Er^{III} ions and four PDA anions. Er1 cation is nine coordinated by eight oxygen atoms from six carboxylate groups and by another water molecule leading to a tricapped trigonal prism geometry. Er2 is octacoordinated by the oxygen atoms of the six carboxylate groups leading to a dodecahedron geometry (Fig. 5a).The Er^{III} ions are further interconnected through the carboxylate groups to form a {Er-OCO} triple helix extending along the crystallographic *c*- direction where two Er ions acting as alternate nodes. The 1D helices (SBUs) are additionally cross-linked by $-CH_2C_6H_4CH_2-$ spacers of the PDA anions resulting in a 3D compressed honeycomb network with 1D open channels when viewed along the crystallographic *c*-axis (Fig. 5b). The guest and coordinated water molecules occupy the channels. The framework showed the high thermal stability and

retention of framework structure with crystallinity upon the removal of guest water molecules to yield $[Er_2(PDA)_3(H_2O)]_n$. The $[\{Er_2(PDA)_3(H_2O)\}\cdot 2H_2O]_n$ framework formed $[Er_2(PDA)_3]_n$ having the same crystalline order and stability as of $[Er_2(PDA)_3(H_2O)]_n$ but here maximized pore volume with a pore dimension of 3.4 Å. Another advantage of such removal of ancillary ligands was that Lewis acidic metal sites were opened up which could assist in higher CO_2 uptake. The framework expectedly showed selective adsorption of CO_2 over N_2 and Ar gas molecules due to a combination of factors such as the difference in kinetic diameters of the gas molecules, dipole-induced dipole interactions and the quadrupolar interaction of CO_2 molecules with the electric field gradient of the framework (Fig. 5c). The authors explained that CO_2 (kinetic diameter = 3.3Å) fit into the pores while N_2 (kinetic diameter = 3.64Å) was not able to fit in. This work showed that it was possible to synthesize stable and porous LOFs with open metal sites for selective capture of gases such as CO_2 over N_2 and Ar.

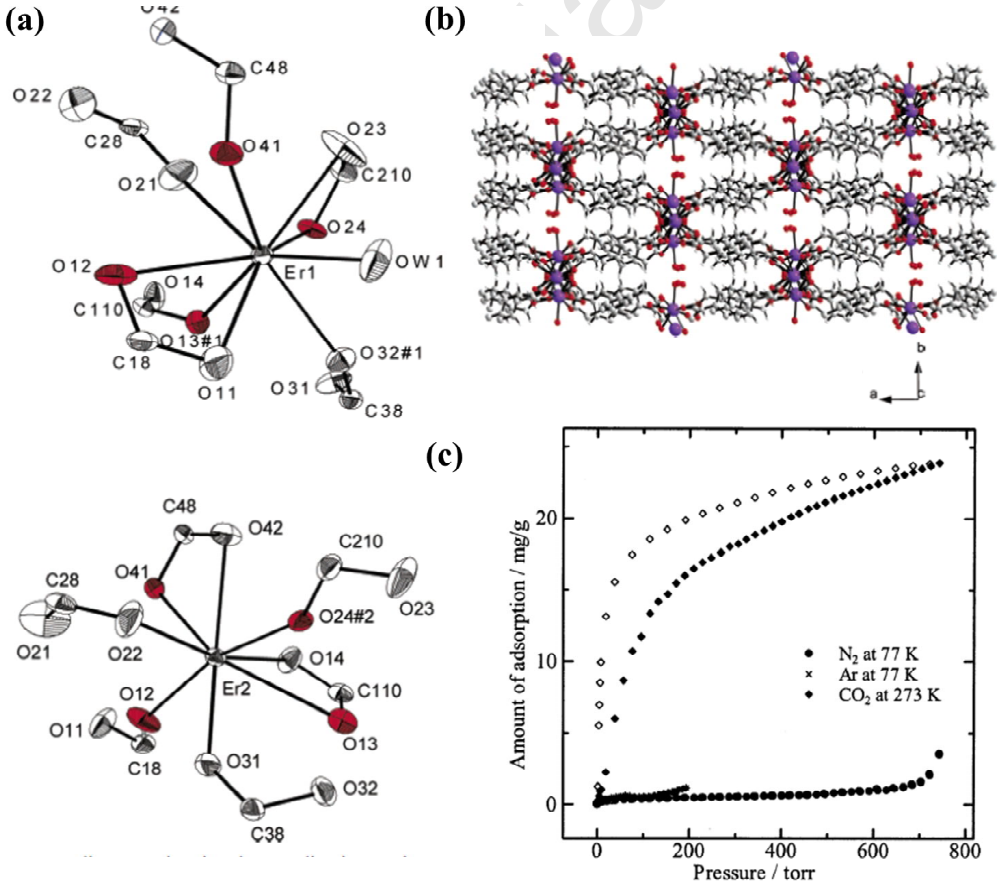

Fig. 5. (a) Coordination environment for Er1 (top) and Er2 (bottom) in $[\{Er_2(PDA)_3(H_2O)\}\cdot 2H_2O]_n$ shown via ORTEP diagrams. Thermal ellipsoids are at 30%

probability. Oxygen atoms in red are coordinated to both Er1 and Er2**.** (b) Illustration of the extended structure of $[\{Er_2(PDA)_3(H_2O)\}\cdot 2H_2O]_n$. Color scheme: Er, blue; O, red; C, gray; H, white**.** (c) Adsorption isotherms of CO_2, N_2, and Ar for $[Er_2(PDA)_3]_n$. The filled and unfilled rhombuses represent adsorption and desorption respectively. Reproduced with permission from Ref. [57]

Kitagawa *et al.* reported two stable porous LOFs $\{[Ln_2(imidc)_2(H_2O)_3](H_2O)\}_n$ (Ln= Gd^{III} and Er^{III}) in 2005 for the selective adsorption of H_2O over MeOH [58]. The frameworks having a zeolite-like topology were stable even upon dehydration and underwent a structural change which allowed the framework to show the selective adsorptive property. The PXRD pattern of the desolvated Gd framework showed appearance of some new peaks when compared to the as-synthesized framework, suggesting some distortion in the structure. The highlighting point in this work was the excellent stability of the lanthanide frameworks which was cultivated for selective adsorption.

In another work, we have demonstrated the structural flexibility and dynamicity of a Gd^{III} framework which could find applications in the selective adsorption of H_2O molecules in a H_2O/MeOH mixture [59]. The crystal structure of $\{[Gd_2(dhbdc)(dhbdcH2)(H_2O)_5]\cdot 2H_2O)\}_n$ (dhbc = 2,5-dihydroxyterephthalate) revealed the presence of two crystallographically unique Gd^{III} centres: one nine coordinated (Gd1) and the other octacoordinated (Gd2), (Fig. 6a). These two Gd atoms are connected by a bridging carboxylate oxygen atom to form Gd-O-Gd chains which are further connected by dhbdc to form 2D corrugated sheets in the crystallographic *ac* plane. These sheets are further pillared by the $dhbdcH_2$ through *syn-syn* bridges between Gd centres to generate a 2D pillared-bilayer network with bidirectional channels along the crystallographic *a* and *c*-axis which are filled with the water molecules. (Fig. 6b). The 2D networks are interdigitated and connected by hydrogen bonding interactions between the coordinated water molecules resulting in a 3D supramolecular framework $\{[Gd_2(dhbdc)(dhbdcH_2)(H_2O)_5]\cdot 2H_2O)\}_n$ with 1D supramolecular channels along the crystallographic *c*-axis (Fig. 6c) . The dimensions of the rectangular and oval shaped pore channels along the *c*-axis are 4.43×3.32 $Å^2$ and 4.43 × 1.94 $Å^2$ respectively whereas along the *a*-axis, the triangular shaped channels have the dimensions of 4.48 × 1.40 $Å^2$. $\{[Gd_2(dhbdc)(dhbdcH_2)(H_2O)_5]\cdot 2H_2O)\}_n$ on partial dehydration yielded $\{[Gd_2(dhbdc)(dhbdcH_2)(H_2O)_5]\}_n$ and $\{[Gd_2(dhbdc)(dhbdcH_2)(H_2O)_4]\}_n$ which showed different sorption ability towards N_2 and also there was more hydrophilicity in the latter framework compared to the former. Interestingly, both the dehydrated frameworks did not

adsorb other solvent molecules such as MeOH, CH_3CN, and EtOH based on size dependent exclusion (Fig. 6d). The N_2 uptake in the latter compound was less compared to the former due to structural contraction on removal of a coordinated water molecule but interestingly, the H_2O sorption data indicated that the latter has a higher affinity for it compared to the former. We attributed this observation to the presence of coordinatively unsaturated Gd^{III} sites which provided a strong interaction with water molecules. MeOH, EtOH and CH_3CN molecules having a higher kinetic diameter than water molecules were unable to penetrate the pore thereby giving rise to selective adsorption of water molecules in the frameworks. Therefore it was seen that dynamicity and flexibility of the Gd framework played an important role in the selective and increased uptake of H_2O molecules over other small solvent molecules.

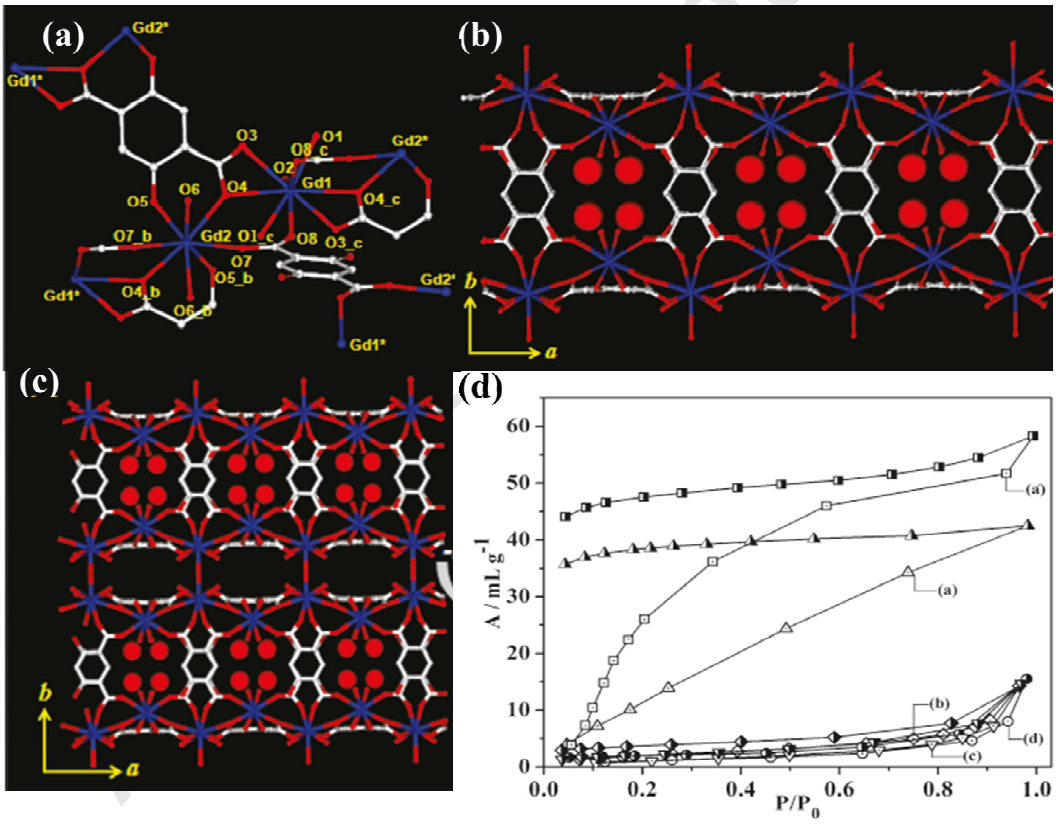

Fig. 6. (a) Structure showing the coordination environments of two Gd^{III} centres in $\{[Gd_2(dhbdc)(dhbdcH_2)(H_2O)_5]\cdot 2H_2O)\}_n$. (b) Structure of the 2D pillared-bilayer framework of $\{[Gd_2(dhbdc)(dhbdcH_2)(H_2O)_5]\cdot 2H_2O)\}_n$ showing water-filled channels along the crystallographic *c*-axis (c) Structure of the interdigitated $\{[Gd_2(dhbdc)(dhbdcH_2)(H_2O)_5]\cdot 2H_2O)\}_n$ formed by the 2D pillared-bilayer framework

showing two different channels along the *c*-axis (d) Sorption isotherms for $\{[Gd_2(dhbdc)(dhbdcH_2)(H_2O)_5]\}_n$ (a) H_2O; (b) MeOH; (c) CH_3CN; and (d) EtOH; (a') H_2O uptake for $\{[Gd_2(dhbdc)(dhbdcH_2)(H_2O)_4]\}_n$. (Curves with half shade symbol correspond to the desorption profile of the respective adsorbates). Reproduced with permission from Ref. [59]

Kitagawa *et al.* recently synthesized a series of LOFs using an acylamide modified ligand (H_3L = 4,4′,4″-(benzenetricarbonyltris-(azanediyl))tribenzoic acid) and $Ln(NO_3)_3{\cdot}xH_2O$ (Ln^{III} = Y, La, Ce, Nd, Eu, Tb, Dy, Ho, and Tm) for effective separation of CO_2 gas from CO_2/C_2H_4 and CO_2/C_2H_6 systems [60]. It was discovered that the flexible nature of the lanthanum framework allowed the selective capture of CO_2 over C_2H_4 and C_2H_6 at an ambient temperature and pressure compared to the other framework structures. Two types of structural topologies of the LOFs were generated and therefore as a representative structural comparison Y^{III}- framework and La^{III}- framework were studied. Both Y and La-framework form 3D structures. In Y- framework, the Y is octacoordinated by seven oxygen atoms from six carboxyl groups and by one DMF molecule whereas in La- framework the La centre is nine coordinated: four oxygens from two chelating carboxyl groups, four bridging oxygens and one DMF molecule. The ligands connect to form an inorganic chain with edge shared polyhedra. In La- framework the chain is slightly helical. In Y- framework, the two adjacent Y atoms are bridged by eight linkers L which are connected to three chains which are in turn linked to six inorganic chains forming the 3D structure. In La- framework on the other hand, nine linkers L bridge two adjacent La centres and these are linked to three helical chains to form the 3D structure. From the structural analysis, it is clear that Y- framework possesses a rectangular channel with a single wall whereas the La-framework possesses a double walled channel having a side by side arrangement of acylamide groups (Fig. 7a). The adsorption experiments carried out at 195K revealed that the La- framework was highly selective for CO_2 whose uptake capacity is ~115 cm^3/g whereas C_2H_4 and C_2H_6 had almost no uptake (Fig. 7b,c). This result showed that La- framework material can be utilized for CO_2 separation in natural gas mixtures. Further CO_2 adsorption studies at 273 K revealed type-I

CO_2 uptake (34 mL/g) at ~150 kPa. Interestingly, before this pressure there was no

adsorption of C_2H_4 and C_2H_6. The excellent practical applicability of this framework therefore lied in the fact that it can separate CO_2 from natural gas mixtures at ambient temperature (273 K) and pressure (0.1-1 bar) and also it can selectively adsorb CO_2 from gas mixtures whereas other materials reported for separation applications adsorb C_2H_6, C_2H_4 over CO_2 [61-63].

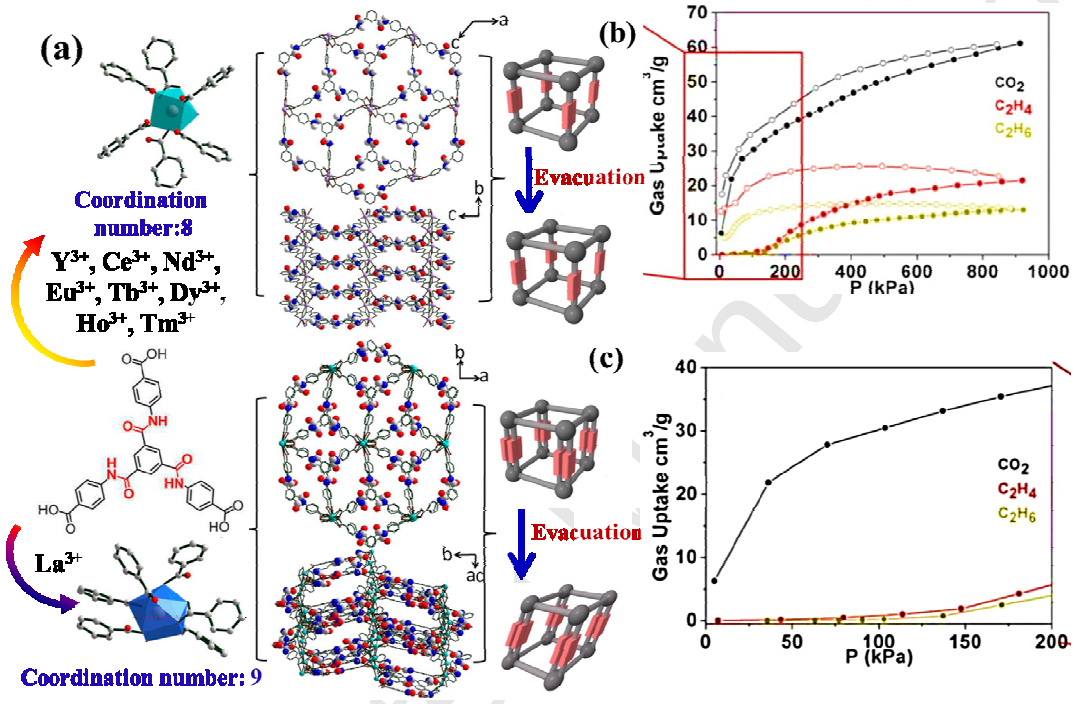

Fig. 7. (a) Scheme showing the coordination environment of different lanthanide ions with L. At the extreme right is shown the likely structural character of the frameworks before and after evacuation. Red spheres represent oxygen, blue spheres represent nitrogen, and gray spheres represent carbon. (b,c) CO_2, C_2H_4, and C_2H_6 uptake in La-framework at 273K. Reproduced with permission from Ref. [60]

3.4. *Luminescent Properties of Lanthanides*

3.4.1. *Theory behind luminescence in lanthanide based systems*

The emission spectral features of lanthanide based compounds are unique because it shows the presence of a large number of weak but sharp bands in the visible region. The sharpness arises due to the occurrence of a large spin-orbit coupling constants that give rise to different J values which are sufficiently separated in energy. Furthermore, the *f*-orbitals are

deep seated and are therefore less prone to interference from the ligand vibrations which make bands appear broad.

The main problem regarding the utilities of lanthanide emission however lies in the fact that the *f-f* transitions like the *d-d* transitions are Laporte forbidden and hence the intensities are very weak and the quantum yields are very low. Nevertheless, a very well-known escape route is provided by what is known as the "antenna effect" [6-10]. This effect is nothing but an energy transfer process from the ligand excited state to the metal excited state and subsequent emission of enhanced intensity from the metal centre is observed [64-66]. A number of factors such as the efficiency of ligand absorption, relative energy states of the ligand and metal and also the efficiency of metal emission play a defining role in this overall process. Upon excitation with UV light, the ligand molecules absorb the radiation and are excited to the higher singlet states ($S_0 \rightarrow S_1$, S_2, S_3…..etc). Two processes can occur from here: it can radiatively decay to the ground state (fluorescence) or it can non-radiatively undergo an inter-system crossing (ISC) to a triplet state. At this triplet state also two molecular processes can occur, i.e it can radiatively decay to the ground state (phosphorescence) or it can transfer its energy to a closely lying lanthanide metal excited state (non-radiative energy transfer). Once this happens, the lanthanide ion can emit the energy and come down to the ground state (Fig. 8).

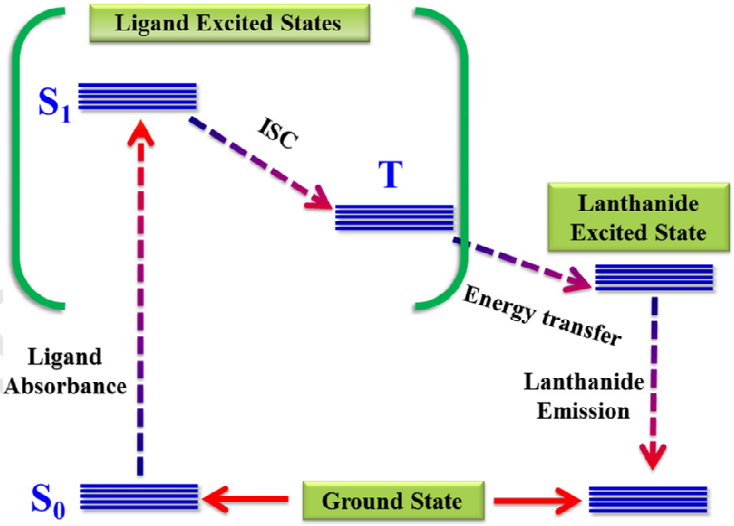

Fig. 8 . A schematic showing the mechanism of lanthanide emission based on the 'Antenna Effect'.

In lanthanide based frameworks the antenna effect has been studied widely. Among the most frequently used linkers are aromatic carboxylate, phosphonate and sulfonates based

ligands [67-72]. Tb^{III} and Eu^{III} metal ions are popularly used for the construction of LOFs and these have intense and line-like luminescence in the green and red regions of the spectrum respectively. Other lanthanide metal ions such as near infra-red emitting Nd^{III}, Yb^{III} and Er^{III} based compounds have also been studied but are less common [73-75]. On analysis of the Eu^{III} complexes spectrum, it is revealed that the $^5D_0$-$^7F_2$ and $^5D_0$-$^7F_1$ transitions are the strongest and most useful for structure determination and sensing application. Also, the $^5D_0$ - $^7F_1$ transition contains a prominent magnetic dipole and is relatively undisturbed by the local environment. However, transitions such as $^5D_0$ - $^7F_2$ in Eu^{III} complexes with $\Delta J = \pm 2$ possessing a strong electric dipole are very much affected by the coordination environment [76]. This inconsistency helps to use relative intensities of these transitions to understand the linker environment. The $^5D_4$ - $^7F_5$ transitions are characteristic of Tb^{III} complexes giving rise to the strong green luminescence at 540–555 nm. In an unprecedented report of co-luminescence in a mixed lanthanide organic framework, Cahill *et al.* showed that a guest mediated antenna effect can lead to selective emission from one particular lanthanide centre [8]. The researchers synthesized a mixed lanthanide framework $[\{(Eu,Tb)(C_6H_8O_4)_3(H_2O)_2\}\cdot(C_{10}H_8N_2)]_n$ ($C_6H_8O_4$ = adipate; $C_{10}H_8N_2$ = 4, 4'-dipyridyl) (Fig. 9a) which showed intense peaks at 595 and 615 nm corresponding to the Eu^{III} and a very weak and almost quenched peak at 545 nm corresponding to the Tb^{III} centre. It is worth mentioning that residual fluorescence from the 4,4'-dipyridyl centred at 475nm, obtained separately from the pure 4,4'-dipyridyl was also completely quenched. This quenching of the guest emission showed that it effectively acts as an antenna and thereby transfers energy to the Tb^{III} centre and also to the Eu^{III} centre. The Eu^{III} centred emission is sensitized by not only the guest dipyridyl molecule but also the Tb^{III} centre (Fig. 9b) as evidenced by the almost complete quenching of the dipyridyl and Tb^{III} emission. This suggests energy transfer from Tb^{III} to Eu^{III} centre. This showed that LOFs showing the antenna effect [77, 78] can be very good systems for luminescence studies and can pave the way for various luminescent applications.

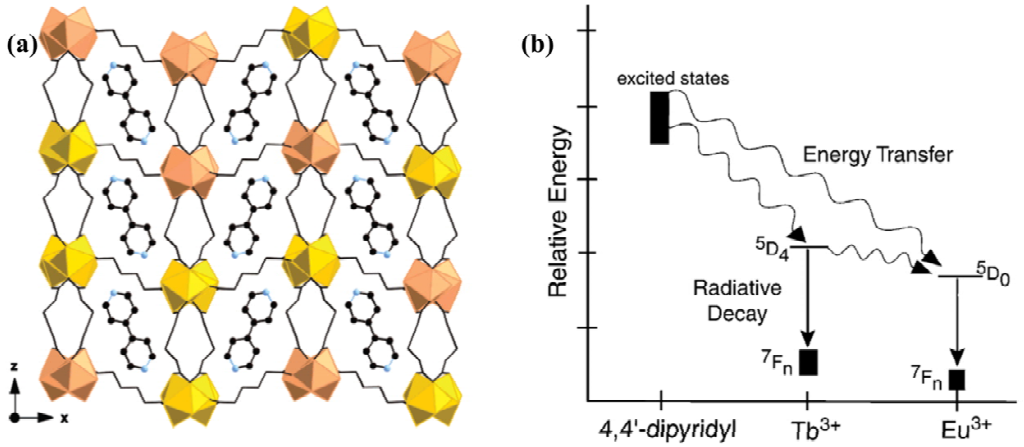

Fig. 9. (a) Crystal structure of $[\{(Eu,Tb)(C_6H_8O_4)_3(H_2O)_2\}\cdot(C_{10}H_8N_2)]_n$ viewed down the [010] direction. The arbitrarily colored polyhedra represent TbO_9 and EuO_9 polyhedra, black lines are adipic acid, and the ball-and-stick figure is 4,4'-dipyridyl (blue denoting the nitrogen atoms**)** (b) The excited state of 4,4'-dipyridyl transfers its energy to the excited state of Tb^{III} and Eu^{III}. The Tb^{III} centre further transfers it energy to the excited state of Eu^{III} thus completely quenching the Tb^{III} emission and enhancing the Eu^{III} emission. Reproduced with permission from Ref. [8]

3.4.2. *Applications of luminescent lanthanide-organic frameworks*

3.4.2.1. *Colour tunabilty and white-light emission*

The last decade and a half has witnessed a sudden spurt in the interest of developing new photo-functional MOFs in various luminescence applications. Integration of lanthanide ions into the framework structures offers an excellent route to cultivate their photoluminescence properties. Colour tunability is one such important feature that leads to white light emission and LOFs provide an excellent opportunity for the exploration of such property. These frameworks exhibit sharp lanthanoid *f-f* emission bands and additionally a broad organic linker based emission. The efficiency of the energy transfer process from the linker to the metal ion then controls the relative intensities of these bands. Furthermore, the emission wavelength can also be tuned in these systems by varying the metal ion concentration, construction of a suitable linker and incorporation of guest species. In general Tb^{III} and Eu^{III} ions are widely used for colour tunability owing to their strong luminescence in the green and red regions respectively. When used together at the same time to form extended frameworks, these form a highly efficient energy transfer pair in which Tb^{III} acts as the donor and funnels excitation energy to the Eu^{III} centre which acts as the acceptor [79-82]. Other

lanthanide ions such as Gd^{III} and Yb^{III} can also be utilized for such colour tunable applications [83, 84].

Rao *et al.* recently reported an unique design strategy for the synthesis of isostructural LOFs doped with Tb^{III} and Eu^{III} [11]. By using the inherent blue emission arising from the ligand centre and varying the Tb^{III} and Eu^{III} concentrations in $[ZJU\text{-}1Tb_xEu_y]_n$ frameworks, it was possible to ultimately generate white light emission at particular concentrations of these two Ln ions. When instead of simultaneous doping, individual metal ions were used, the characteristic emission features of that particular metal ion were obtained. Thus, $[ZJU\text{-}1Tb^{3+}]_n$ on excitation at 312 nm showed characteristic peaks at 490, 543, 585 and 622 nm for Tb^{III} corresponding to the transitions between the first excited state ($^5D_4$) and the ground multiplet (^7F_J, = 6–3) and also an emission at 408 nm from the ligand. Similarly $[ZJU\text{-}1Eu^{3+}]_n$ on excitation at the same wavelength, in addition to the ligand emission peak, showed characteristic Eu^{III} emission peaks at 580, 592, 614, 650 and 694 nm assigned to the transitions between the first excited state ($^5D_0$) and the ground multiplet (^7F_J, J = 0–4). This proved that an efficient energy transfer process was occurring between the ligand centre and the individual metal ions. Therefore when both the metal ions were present simultaneously based on doping, the tuning of emission colour through an energy transfer process was observed. Interestingly, at optimum concentrations of Eu^{III} and Tb^{III} doping ($[ZJU\text{-}1Tb_{1\%}Eu_{2\%}]_n$ and $[ZJU\text{-}1Tb_{1.5\%}Eu_{2\%}]_n$) pure white light with CIE coordinates of (0.3269, 0.3123) and (0.3109, 0.3332) respectively were generated. This paper showed that a simple approach of doping in porous lanthanide frameworks can effectively tune the emission wavelength of the framework over an extensive range and also a balanced concentration of doped metal ions can help to generate white light from the material. The fascinating energy transfer phenomenon between the Tb^{II} and Eu^{III} pair of lanthanide ions has also been utilized in another interesting work by Liu *et al.* for generating white light by co-doping these metal ions into a blue-emitting lanthanide-organic framework [12].

Recently our group exploited the donor-acceptor ability of the Tb^{III}-Eu^{III} pair in effectively tuning the emission colour of Tb^{III}-mucicate frameworks [85]. Two different 3D compounds $\{[Tb_2(Mu^{2-})_3(H_2O)_2]\cdot 4H_2O\}_n$ (Tb-1) and $\{[Tb(Mu^{2-})\text{-}(Ox^{2-})_{0.5}(H_2O)]\cdot H_2O\}_n$ (Tb-2) were obtained under solvothermal condition by varying the pH of the medium (Fig. 10 a,b). Further, a Eu^{III} mucicate compound isomorphous to Tb-1 was synthesized under similar reaction condition. Tb-1 and Tb-2 show 1D water filled channels and reveal strong hydrophilic pore surfaces. The emission properties of Tb-1 and its Eu^{III}-analogue were

studied in detail. The Tb-1 framework showed characteristic peaks at 485, 545, 585, and 620 nm assigned to $^5D_4$-to-^7F_J transitions, where J= 6-3, respectively whereas the peaks for the Eu^{III} framework was shown to be at 590, 615, 650, and 693 nm attributed to $^5D_0$-to-^7F_J transitions, where J= 1−4, respectively. The Tb-1 framework showed green colour due to the presence of the intense peak at 545nm whereas the Eu^{III} framework demonstrated strong red emission due to the 615 nm peak. Exploiting the fact that Tb^{III} and Eu^{III} form a very good donor-acceptor pair and that also their charge and ionic radii match, we had doped controlled amounts of Eu^{III} (Eu^{3+}= 50, 24, 15, 7, 4, 1.24, and 0.6 atom %) into the Tb-1 framework and observed emissions ranging from green to red (Fig. 10c). The spectra of the different doped compounds: $\{[Tb_{2-2x}Eu_{2x}(Mu^{2-})_3(H_2O)_2]\cdot 4H_2O\}_n$ show peaks at 485, 545, 589, and 615 nm with the highest intense peaks at 545 and 615 nm corresponding to green and red emission. As expected the intensities of the peaks at 545 and 615 nm increased and decreased respectively as the doping concentration of Eu^{III} increased (Fig. 10c). The indisputable proof that Försters resonance energy transfer was indeed occurring between Tb^{III} to Eu^{III} in doped compound was the lifetime of the ground state terms $^5D_4$ of Tb^{III} and $^5D_0$ of Eu^{III} that showed a decrease and increase in the decay profile when compared to the original Tb-1 framework and its Eu^{III} analogue. This work thus provides an insight into the interesting chemistry of Tb^{III} and Eu^{III} lanthanide ions that allows us to exploit their emission characteristics into effective colour tuning in the visible light.

The greatest challenge in the practical applicability of these porous coordination polymers is solution processability in the bulk scale. For practical uses of these luminescence properties, the materials must possess the physical properties that enable them to be used for device fabrication. Nanoscale synthesis of these materials therefore offers a gateway for the practical application of such materials. In the nanodomain, the individual particles are well dispersed and thus the material at the nanoscale becomes easier to coat onto other high surface area materials. One such work of generating metal coordination polymers at the nanoscale was reported by Zhong *et al.* [13]. In this study they explored the versatile luminescent behaviour of a novel $[Tb\text{-}BTB]_n$ (BTB = 4,4',4''-benzene-1,3,5-triyl-tri-benzonate) infinite coordination polymer (ICP) on doping with different percentages of Eu^{III}. Interestingly white light emission was made possible in this hybrid system by tuning the emission colour via this doping method. Upon excitation at 316nm, the emission spectra consisted of a broad ligand based emission band at 388 nm and four sharp Tb^{III} based emission bands at 487, 543, 581, and 619 nm corresponding to the $^5D_4$-^7F_J (J=6, 5, 4, and 3,

respectively) transitions. When the concentration of Eu^{III} ions were increased in Tb-BTB-1:xEu^{III} from x=0.05% to 10% a gradual shift in emission colour was observed from blue-green to red. White-light emission was observed when the doping concentration reached 0.5% which renders this ICP a good candidate as a white light source.

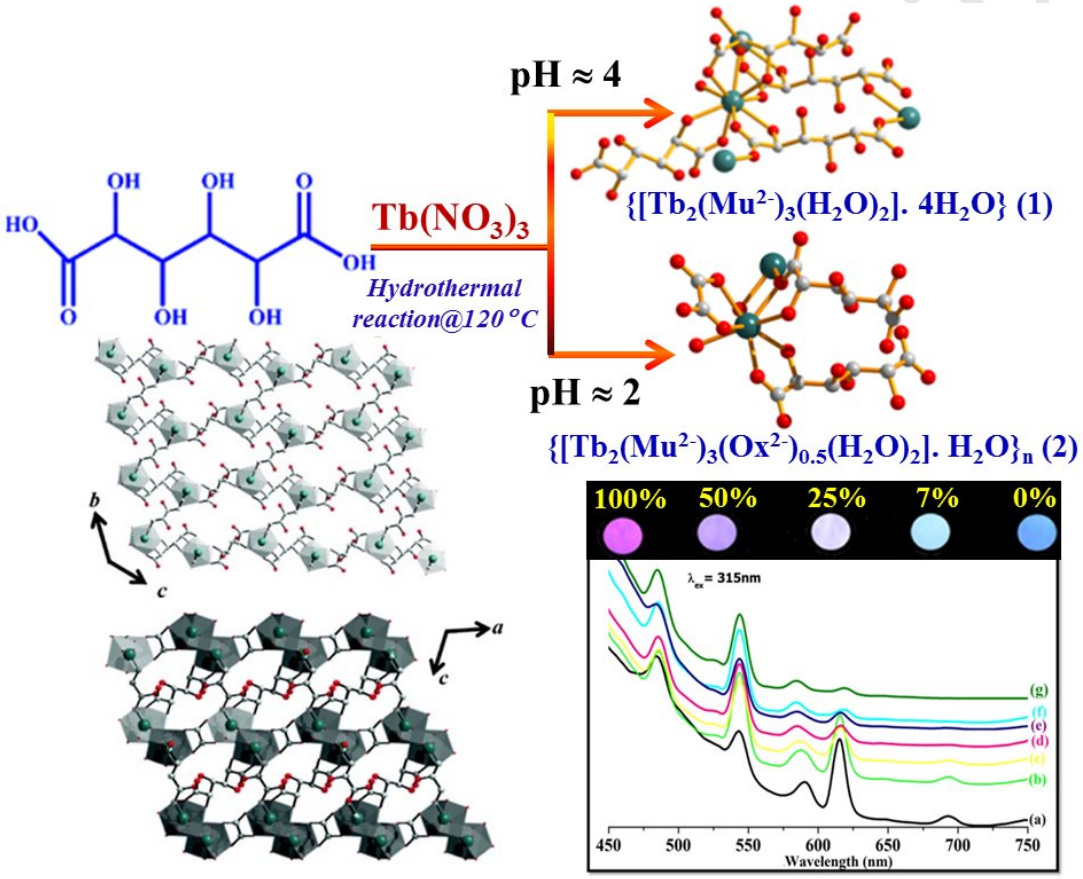

Fig. 10. (a) Scheme depicting a pH-controlled synthesis of $\{[Tb_2(Mu^{2-})_3(H_2O)_2]\cdot 4H_2O\}_n$ (Tb-1) and $\{[Tb(Mu^{2-})\text{-}(Ox^{2-})_{0.5}(H_2O)]\cdot H_2O\}_n$ (Tb-2). (b) 3D structure of $\{[Tb_2(Mu^{2-})_3(H_2O)_2]\cdot 4H_2O\}_n$ formed by the three different binding modes of Mu^{2-} viewed along the *a*-axis and 3D structure of $\{[Tb(Mu^{2-})(Ox^{2-})_{0.5}(H_2O)]\cdot H_2O\}_n$ viewed along the *b*-axis and formed by two different Mu^{2-} and one Ox^{2-}. (c) (Top) Samples of different Eu^{III} contents in $\{[Tb_2(Mu^{2-})_3(H_2O)_2]\cdot 4H_2O\}_n$ showing different colours under UV light. (Bottom) Emission spectra of mixed Tb^{III}–Eu^{III} compounds with different percentages of Eu doping (λ_{ex} = 315 nm): (a) 50%; (b) 24%; (c) 15%; (d) 7%; (e) 4%; (f) 1.24%; (g) 0.6%. Reproduced with permission from Ref. [85]

Another interesting work that needs to be highlighted is heterometallic coordination polymer reported by Liu *et al*. In this work they have systematically synthesized a compound $[\{EuAg_3(3\text{-}TPyMNTB)_2(H_2O)(MeCN)\}(ClO_4)_6\cdot 4MeCN]_n$ (2-Eu-Ag) from the self-assembly of a pre-synthesized Eu^{III} monomeric complex $[Eu(3\text{-}TPyMNTB)_2](ClO_4)_3\cdot 2.5MeCN$ (1-Eu) and $AgClO_4$. (Fig. 11a) [14]. The monomeric complex showed the antenna effect to generate red light whereas the addition of the silver ions helped in the generation of white light in the compound via the resensitization of the ligand based emission by the silver ion. The ligand showed weak emission peaks at 530 nm and another shoulder at 375 nm. In 1-Eu, the ligand emission was reduced due to the ligand to Eu^{III} energy transfer based on antenna effect and thus strong Eu^{III} based emission was observed. On the other hand, 2-Eu-Ag showed a different emission spectral profile from 1-Eu. The emission from the ligand was observed here along with the characteristic emission from the Eu^{III} centre. This happened due to the resensitization of the ligand emission by the silver ions (Fig. 11b) as the silver ions help in making the structure more rigid and an intra-ligand $^1\pi\pi^*$ singlet transition which resensitized the ligand emission. The combination of the ligand and the Eu^{III} based emission in 2-Eu-Ag was effective in generating white-light emission form this heterometallic compound. Another interesting feature of this heterometallic luminescent framework was that the emission colour was tunable by changing the excitation wavelength from 310 to 370 nm generating CIE coordinates from (0.42, 0.32) to (0.45, 0.37), all falling within the white- light region. This result suggests that the white-light emission is also dependant on the excitation wavelength and the emission colour of such dual emissive frameworks can be tuned by changing the excitation wavelength.

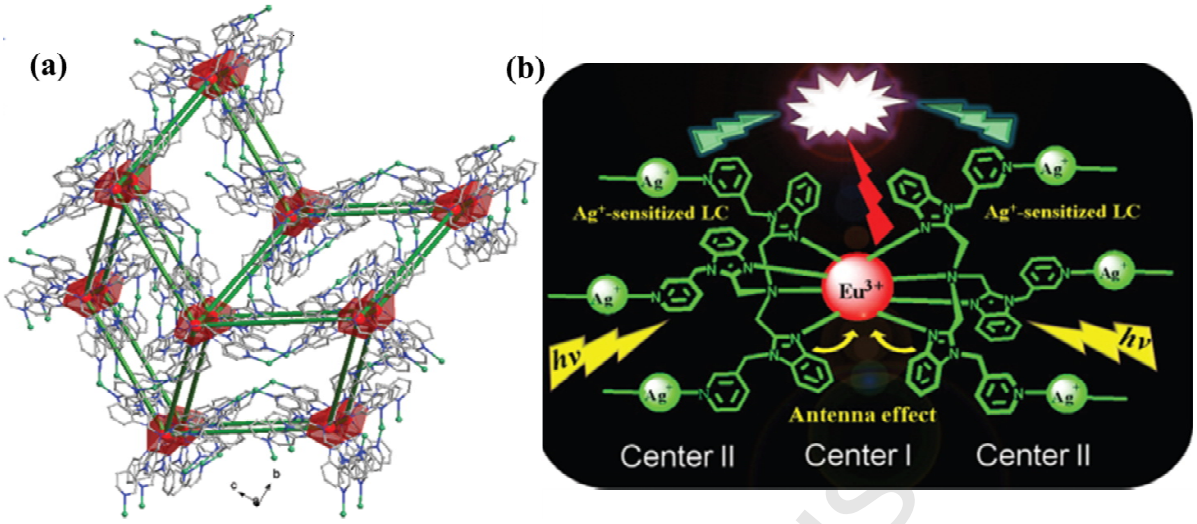

Fig. 11. (a) 3D structure of $[\{EuAg_3(3TPyMNTB)_2(H_2O)(MeCN)\}(ClO_4)_6 \cdot 4MeCN]_n$ showing pcu topology represented by green solid lines**.** (b) Schematic showing the resensitization of the ligand emission by silver ions generating white light from the heterometallic framework $[\{EuAg_3(3TPyMNTB)_2(H_2O)(MeCN)\}(ClO_4)_6 \cdot 4MeCN]_n$ Reproduced with permission from Ref. [14]

3.4.2.2 Sensing applications

The permanent porosity and luminescent property of LOFs can be cultivated for a variety of applications like chemical sensing, optoelectronic properties, biomedical imaging and photocatalytic applications. Moreover, these lanthanide frameworks when prepared at the nanoscale can be utilized in cell and tissue imaging applications and drug delivery as their size would permit their entry into living cells. Over the last few years, a number of luminescent LOFs have been developed for sensing of cations, anions, small organic molecules and even gas vapours. These sensing properties have been explored based on the change of luminescence properties of the host with different analytes. The structural backbone of the framework, permanent porosity, nature of pore surfaces play important role for reversible uptake and release of guest molecules within the framework through supramolecular interactions. Also the presence of unsaturated lanthanide centres within the pores can enhance the reversible uptake of specific anions required for their sensing.

3.4.2.2.1. *Cation Sensing*

The year 2004 saw the first report of a lanthanide framework being used as a sensor for cations. Liu *et al.* synthesized a 3D framework $\{Na[EuL(H_2O)_4]\cdot 2H_2O\}_n$ for effective

sensing of Ag^{I} cations [86]. The *d*-block cations occupied the empty coordination site of the tetraazacycle of the ligand in the complex (Fig. 12a). It was observed that Cu^{II}, Zn^{II}, Cd^{II}, and Hg^{II} ions quenched the Eu^{III} complex emission. Interestingly, Ag^{I} ions can enhance the emission along with the reduction in the number of emission lines the complex. The intensity of the single emission peak ($^5D_0$ - $^7F_2$ transition) in the Ag^{I} containing complex was enhanced 4.9 times as shown in the Fig. 12b, suggesting the potential of this framework for Ag^{I} sensing.

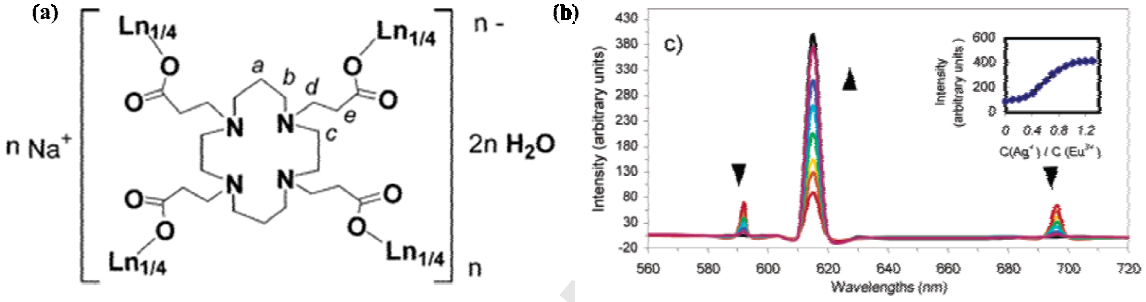

Fig. 12 (a) Schematic structural representation of the complex $\{Na[EuL(H_2O)_4].2H_2O\}_n$ (Ln= Eu^{III}). (b) Graph showing the increase in luminescence intensity of a 1.0×10^{-4} M solution of complex in H_2O upon addition of Ag^{I}. Inset: luminescence intensity at 615 nm against the mole concentration ratios $C(Ag^{I})/C(Eu^{III})$ plot; the line represents the fit to a 1:1 binding model. Reproduced with permission from Ref. [86]

Zhao *et al.* reported the sensing of Zn^{II} ion using frameworks $\{[Ln(PDA)_3Mn_{1.5}(H2O)_3]\cdot3.25H_2O\}_n$ with 1D channels (PDA= pyridine-2,6-dicarboxylate). (Ln = Eu (**1**); Tb (**2**)) [87]. Both these frameworks showed an increase in emission intensity on incorporation of Zn^{2+} whereas other cations such as $Mn^{II,}$ Ca^{II}, Mg^{II}, Fe^{II}, Co^{II}, and Ni^{II} showed unchanged or weakened emission spectra upon incorporation. It was attributed to the fact that Zn^{II} ions enhance the effectiveness of the intramolecular energy transfer process from the PDA ligands to the lanthanide ions. This result showed that design of porous lanthanide frameworks for the selective sensing of Zn^{II} over other *d*-block metal ions is achievable.

An interesting approach towards the sensing of metal cations was put forward by Chen *et al.* [88]. Here they utilized the greater coordinating preference of Ln ions towards carboxylate oxygen donor sites than nitrogen donor sites of pyridine dicarboxylate based

linkers. A LOF $[\{Eu(pdc)_{1.5}(dmf)\}\cdot(DMF)_{0.5}(H_2O)_{0.5}]_n$ was synthesized via a solvothermal route and structural analysis showed that the Eu^{III} ions were bound to the carboxylate oxygen atom of the pdc ligand leaving the pyridyl nitrogen free. The framework with Lewis basic pyridine sites decorated on the pore surfaces has been exploited for metal ion sensing based on Lewis acid-base interaction (Fig. 13a). A large number of metal cations were studied (Na^{I}, K^{I}, Mg^{II}, Ca^{II}, Mn^{II}, Co^{II}, Cu^{II}, Zn^{II}, Cd^{II}) and it was observed a marked decrease in fluorescence intensity was occurring for Cu^{II} over other alkali and alkaline-earth metal ions as indicated in Fig. (13b, c). The authors put forward the explanation that alkali metal ions do not bind to the free pyridyl nitrogen and hence have no effect on deactivation of the antenna effect to reduce the fluorescence intensity. On the other hand, Cu^{II}, Co^{II} and Mn^{II} can bind to the free pyridyl nitrogen and has the effect of reduction on the antenna effect efficiency of the pdc linker thereby reducing the overall fluorescence intensity of the Eu^{III} centre.

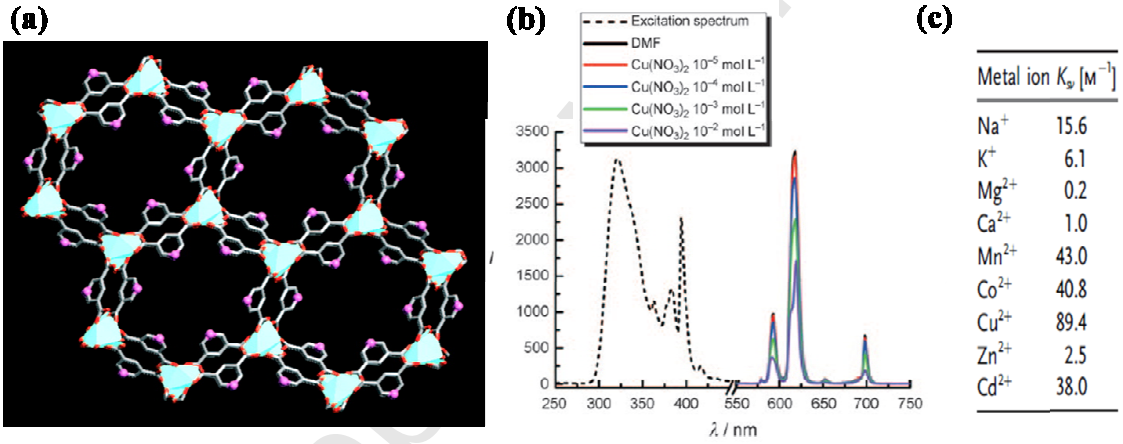

Fig. 13. (a) Crystal structure of $\{[Eu(pdc)_{1.5}(dmf)]\cdot(DMF)_{0.5}(H_2O)_{0.5}\}_n$ with fixed Lewis basic pyridyl sites oriented towards pore, viewed along the crystallographic *a* axis (C grey, N purple, O red, Eu green polyhedral) (b)The excitation (dotted lines) and PL spectra (solid lines) of activated $[\{Eu(pdc)_{1.5}\}\cdot DMF]_n$ in DMF solutions of $Cu(NO_3)_2$ at different concentrations. (c) Quenching effect coefficients (K_{sv}) of different metal ions on the luminescence intensity of metal-ion-incorporated $\{[Eu(pdc)1.5]\cdot DMF\}_n$. Reproduced with permission from Ref. [88]

3.4.2.2.2. Anion sensing

Anions also play a pivotal role in biological and environmental systems [89-92] and therefore development of techniques for their sensing is a challenging problem to be

addressed. It is a well-known fact that the stretching vibrations of the –OH groups of water molecules have a quenching effect on the emission intensity of the metal centres in lanthanide complexes [93]. The water molecules in LOFs give rise to reduced fluorescence intensity and therefore the emission intensity should be enhanced upon the removal of the water molecules. This effect was demonstrated by Wong *et al.*in their mucicate based lanthanide framework $\{[Tb(Mucicate)_{1.5}(H_2O)_2]\cdot 5H_2O\}_n$ [94]. They proposed that this compound would act as an efficient anion sensor due to intermolecular hydrogen bonding between the negatively charged anion centre with the hydrogen of water molecules thereby increasing the emission intensity due to the suppression of –OH vibrations. A host of anions such as I^-, Br^-, Cl^-, F^-, CN^-, and CO_3^{2-}, SO_4^{3-} and PO_4^{3-} were studied .The effect was found largest for the CO_3^{2-} anion whereas for larger anions like SO_4^{3-} and PO_4^{3-}, no such luminescence enhancements were observed (Fig. 14). This was attributed to the inability of these large anions to penetrate the channels. This work shows that lanthanide frameworks with hydrophilic pore channels can act as an effective material for the sensing of anions via the suppression of the –OH vibrational modes through intermolecular hydrogen bonding.

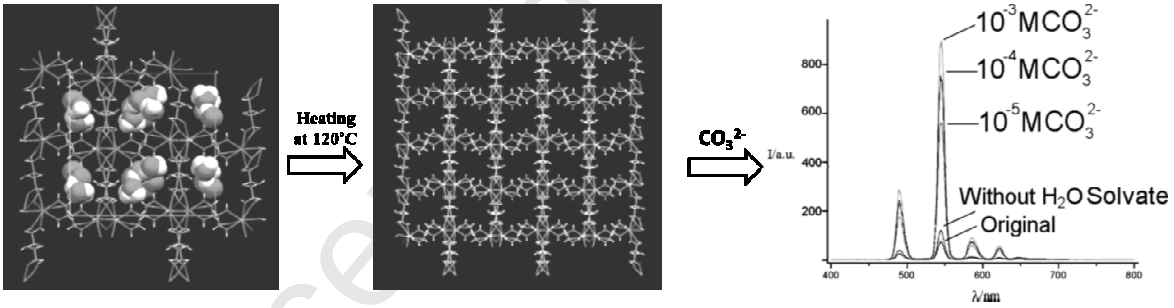

Fig. 14. Left and center: framework structures of $\{[Tb(Mucicate)_{1.5}\text{-}(H_2O)_2]\cdot 5H_2O\}_n$ before and after the removal of water respectively. Right: Plot showing the luminescence spectra of $\{[Tb(Mucicate)_{1.5}\text{-}(H_2O)_2]\cdot 5H_2O\}_n$ with and without water and at various concentrations (10^{-3}–10^{-5} M) of CO_3^{2-}. Reproduced with permission from Ref. [94]

Other anion sensing LOFs have also been reported. One such work is demonstrated by Chen *et al.* where the authors have shown that the framework $\{Tb(btc)\cdot G\}_n$ (MOF-76) with terminal methanol molecules is a very good material for F^- sensing. The anions like F^-, Cl^-,

and Br^- suppress the vibrational modes of the –OH group of methanol molecules through intermolecular hydrogen bonding (Fig.15a) [95]. The fluorescence enhancement was found to be maximum for F^- with approximately a four times increase when compared to that of the non F^- incorporated MOF-76 (Fig. 15b). This was due to the stronger hydrogen bonding interactions between the F^- anions with the terminal methanol molecules.

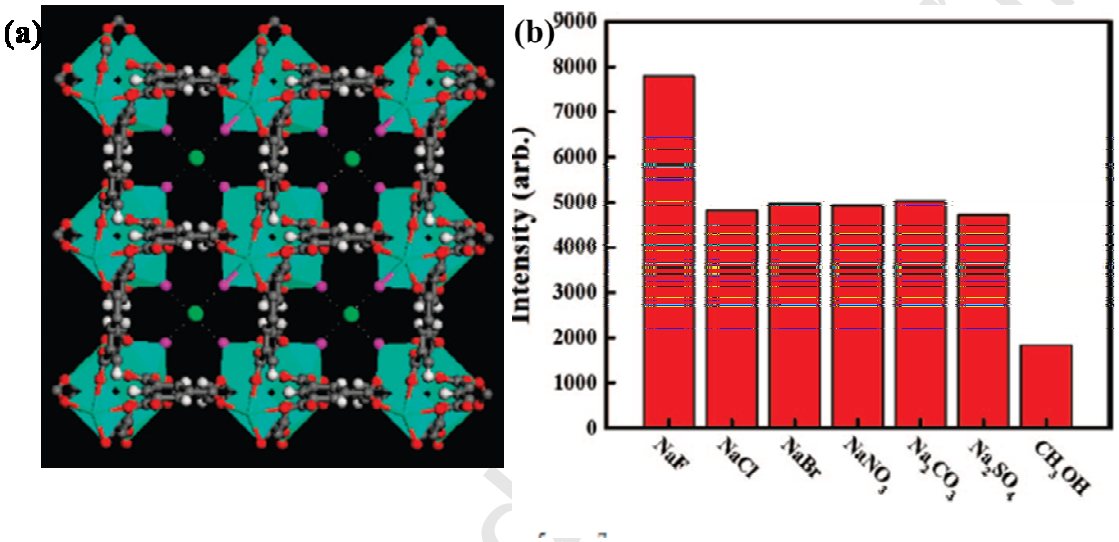

Fig. 15. (a) Single crystal X-ray structure of MOF-76b activated in methanol containing NaF showing the hydrogen-bonding interaction of model fluoride (green) with the terminal methanol molecules (methanol oxygen, purple). (b) Plot showing the variation of the $^5D_4$-$^7F_5$ transition intensities of MOF-76b activated in different types of 10^{-2} M NaX and Na_2X methanol solution (excited and monitored at 353 and 548 nm, respectively). Reproduced with permission from Ref. [95]

3.4.2.2.3. *Sensing of small molecules*

The luminescence of LOFs can also be utilized for sensing small molecules and explosives. Chen *et al.* synthesized a Eu^{III} based framework $\{Eu(BTC)(H_2O)\cdot 1.5H_2O\}_n$ (Fig. 16a) which was isostructural with MOF-76 [96]. The activated structure contains open Eu^{III} sites which can be utilized for sensing small molecules. Its potential applications in sensing was realised in solvent emulsion phases with different solvents. DMF and acetone exhibited the maximum enhancing and quenching effects respectively (Fig.16b). The authors however have not given a confirmatory mechanism of the fluorescence enhancement and quenching by

the solvent molecules. It is predicted that the dispersion of the compound in isopropanol solvent contains the isopropanol molecules coordinated to the Eu^{III} sites. These coordinated isopropanol molecules are gradually replaced by the DMF and acetone molecules when the Eu^{III} compound was dispersed in the particular solvent. This causes the enhancement and decrease of fluorescence observed in the framework emission when exposed to these solvent molecules.

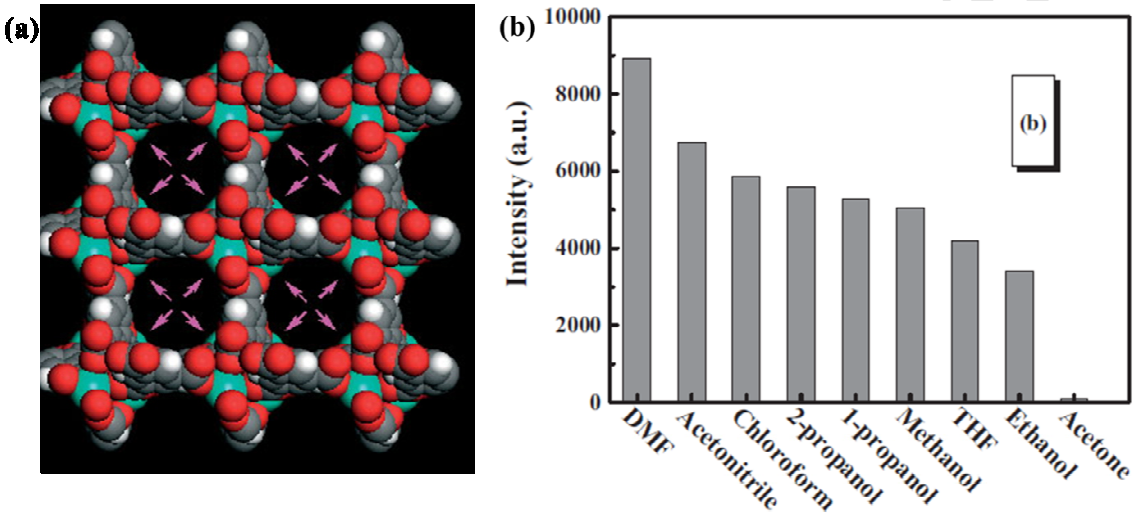

Fig. 16. (a) View of the three dimensional framework of $\{Eu(BTC)(H_2O)\cdot 1.5H_2O\}_n$ along the *c*-axis, having 1D channels of about 6.6 × 6.6 Å, and uniformly immobilized accessible Eu^{III} sites within the framework (indicated by the pink arrows). The free and terminal water molecules are omitted for clarity; Eu, light green; O, red; C, grey; H, white. (b) Plot showing the variation of the $^5D_0 \rightarrow {}^7F_2$ transition intensities (λ_{ex}: 285nm) of $\{Eu(BTC)(H_2O)\cdot 1.5H_2O\}_n$ when introduced into various pure solvents. Reproduced with permission from Ref. [96]

Ma *et al.* were also successful in synthesizing a Eu^{III} based framework $[\{Eu_2(\mu_2\text{-}pzdc)(\mu_4\text{-}pzdc)(\mu_2\text{-}ox)(H_2O)_4\}\cdot 8H_2O]_n$ that could be used as a sensor for acetone [97]. The desolvated framework was immersed in different organic solvent emulsions and the corresponding solvent induced change of Eu^{III} emission was observed. The PL spectra showed that methanol had negligible effect on the emission whereas acetone had the maximum quenching effect on the emission profile. On progressive addition of acetone, at 5.75 vol % complete quenching of Eu^{III} emission was observed. Under similar experimental conditions, other solvent molecules displayed intermediate quenching effects. It was then concluded that small solvent molecules effectively quench the energy transfer process from

the ligand to the Eu^{III} centre. Unlike the previous work, the metal is not unsaturated and hence guest solvent molecules were interacting with some other site in the framework. There have been other reports of LOFs for active sensing of small molecules which expand the practical utility of such lanthanide based systems [98-101].

Nanoscale framework materials have excellent dispersability in various solvents and this gives them the advantage of direct interaction with molecules without the activation step being performed. One such nanoscale lanthanide compound $\{[Eu_2(bdc)_3(H_2O)_2]\cdot(H_2O)_2\}_n$ was prepared by Xu *et al*. and used for selective sensing of nitroaromatics such as nitrobenzene, 2,4-dinitrobenzene and 2,4,6-trinitrobenzene along with other analytes [102]. 150 ppm of the analytes when added to a dispersed solution of the Eu^{III} compound in ethanol showed a marked decrease in luminescence intensity compared to the original framework selectively for the nitro-explosives. The explanation given by the authors is that the analyte molecule competes with the bdc ligand for absorption of light energy and hence reduces the amount of light absorbed by the ligand thereby reducing the efficiency of energy transfer from the ligand to the lanthanide metal centre. The electronic interaction between the analyte molecules and the bdc molecules also play a role in this fluorescence quenching. This study demonstrates that nanoscale lanthanide frameworks with a variety of organic linkers which have matching competitive absorptions with explosive analyte molecules can be utilized as sensors of explosives.

A very interesting work on the sensing of ferrocene molecules was reported by Park *et al.* in a Tb^{III} based mesoporous framework $\{[Tb_{16}(TATB)_{16}(DMA)_{24}]_3(DMA)_{91}(H_2O)_{108}\}_n$ (Fig 17a) [103]. In this work they have observed that the sharp and line like green emission from the Tb^{III} centre was changing to a weak and broad emission on incorporation of ferrocene molecules within the pores. This observation was attributed to the phenomenon of efficient energy transfer from the host framework to the ferrocene molecules whose absorption overlaps with the emission of the framework. Interestingly, when the guest ferrocene molecules were removed under heating and vacuum, the green emission from the host framework was recovered and with the disappearance of the ferrocene emission (Fig. 17b). This reversible change of luminescence via the reversible uptake and release of ferrocene molecules allows this mesoporous framework to effectively sense it.

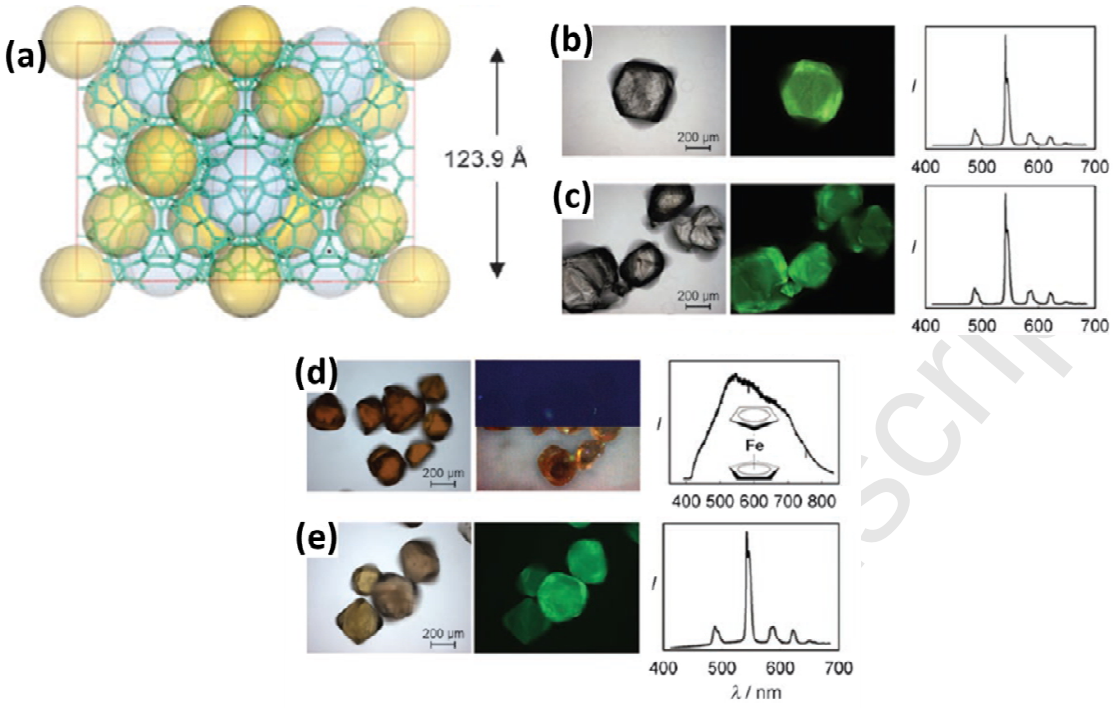

Fig. 17. (a) Structure of a cubic unit cell of $\{[Tb_{16}(TATB)_{16}(DMA)_{24}]_3(DMA)_{91}(H_2O)_{108}\}_n$ viewed along the [101] direction. The large and small spheres represent the inner spaces of the mesocages, and the sticks connect the Tb^{III} ions (b) Microscope images of a crystal of 1 taken in transmission mode (left) and in fluorescence mode (middle), and its luminescence spectrum (right). (b) As in (b), for a bulk sample. (c) As in (b), for ferrocene-containing crystals. (d) As in (b), for the crystals used in (c) after evacuation at 50˚C for 1 day. Reproduced with permission from Ref. [103]

4. Magnetism in Lanthanide –Organic Frameworks

One of the most fundamental properties of materials is magnetism and study of different magnetic properties in metal-organic frameworks has been a fascinating research aspiration. In lanthanide (Ln) based molecular materials, the magnetic properties are often very interesting and complex at the same time. Indeed, the nature of magnetic coupling between Ln ions still remains a topic being far from satisfactorily understood. Despite their complexity, lanthanide based hybrid compounds has attained considerable research interests to the chemists and materials scientists owing to their certain features such as high anisotropy, resulting slow relaxation of magnetization. Especially, synthesis and study of the SMMs [104-113] and single-chain magnets (SCMs) [114,115] based on lanthanide system represents a very attractive research field as these compounds can serve potential applications

in high-density data storage technologies and molecular spintronics [116]. SMMs based on lanthanides have been extensively studied over the past few years. Here in this review, we will restrict our discussion only on higher-dimensional frameworks [117-122]. Similar to the zero-dimensional cluster, in 3D LOFs, slow relaxation can occur because of the anisotropy of the systems, while quantum tunnelling is unlikely because of the bulk 3D structure. In Ln-organic frameworks, single-ion anisotropy of the metal ion results strong easy-axis type anisotropy. The slow relaxation of the magnetization is a result of this uniaxial anisotropy of the molecule, which ensues the direction of the molecular magnetization to be fixed. Indeed, this single-ion anisotropy and the large *J(L+S)* value of the Ln ions have resulted fabrication of many excellent Ln-based magnetic compounds. In addition to the effect of slow relaxation of magnetization, the succeeding discussions of this review will focus on different type of magnetic interaction and guest induced change in magnetic behaviour in 3D LOFs.

4.1 *Different magnetic interaction in Ln-based frameworks (ferromagnetic and antiferromagnetic interaction)*

The magnetic interactions between Ln ions involving the f electron pairs are weak and often masked by the crystal field effect on the magnetic susceptibility. Thus analysis of the data of lanthanide system becomes usually difficult. Despite this difficulty, chemists have been continuing their effort to explore such system revealing interesting magnetic behaviour. Specially, the unquenched orbital moment of Ln ions can give rise to fascinating properties associated with their anisotropy. However, the description and interpretation of magnetic properties of Gd^{III} (f^7) system remain easier because of no orbital momentum. Generally, the interaction between adjacent Gd^{III} ions is antiferromagnetic in nature [118, 119] and only a few Gd^{III}-based frameworks with different carboxylate building block have shown ferromagnetic interaction [117]. Many other Ln-organic frameworks largely display antiferromagnetic interaction [120] and often exhibit gradual decrease in $\chi_M T$ value with gradual decrease in temperature due to the depopulation of Stark level, which can be overcome by the ferromagnetic interaction in certain compounds. Though the detailed investigations of origin of complex magnetic interactions have yet to be properly studied, a handful of literature reports are available documenting different magnetic interactions. These reports mainly include antiferromagnetic compounds while the occurrence of ferromagnetism has been reported to a lesser extent. We will be presenting some such examples of different interaction in Ln-based framework materials.

Weng *et al.* have [31] reported a series of compound with the formula $[Ln(pza)(OH)(H_2O)]_n$ (pza = 2,3-pyrazinedicarboxylate, Ln = Y(**1**), Er(**2**), Yb(**3**); extended by 2,3-pyrazinedicarboxylate. The compounds are isostructural and they contain layered two-dimensional net consisting of centrosymmetric $M_2(\mu_2\text{-}OH)_2$ units, where the dinuclear $M_2(\mu_2\text{-}OH)_2$ clusters are bridged by pza ligands resulting a neutral 2D grid lying in the (100) plane. The $M_2(\mu_2\text{-}OH)_2$ core can be considered as a six-connected node while the pza ligand can be considered as a three-connected linker. Topological investigation reveals that the 2D network can be represented with the Schläfli symbol $(4^3)_2(4^6,6^6,8^3)$ (Fig. 18a). The 2D networks are further assembled via H-bonds and the π–π stacking of pyrazine rings forming a supramolecular 3D framework (Fig. 18b). The Er^{III} compound shows ferromagnetic interaction which is clear from its $\chi_M T$ *vs*. *T* plot (Fig. 18d) and positive θ value. The Yb^{III} compound exhibits decrease in $\chi_M T$ with decrease in temperature (Fig. 18e) and negative θ value suggesting depopulation of the Stark levels of the Yb^{III} ions together with a possible weak antiferromagnetic coupling. The possible antiferromagnetic interaction was ascribed to the Yb^{III}-Yb^{III} interaction through the hydroxo bridge. Thus diverse magnetic interactions were documented in a family of isostructural structures by changing only the Ln^{III} ions.

Another family of isostructural lanthanide-organic coordination polymers formulated as $\{[Ln_2(Hpimda)_2(\mu_4\text{-}C_2O_4)\cdot 2H_2O]\cdot 4H_2O\}_n$ (H_3pimda = 2-Propyl-1H-imidazole-4,5-dicarboxylic acid, Ln = Sm (**1**), Eu (**2**), Tb **(3)**, Dy (**4**), Ho (**5**), Er (**6**), were furnished by the self-assembly of 2-Propyl-1H-imidazole-4,5-dicarboxylate and oxalate [121]. The structural aspect of Sm^{III} compound (**1**) is described to illustrate the structures of the isostructural frameworks. The coordination polyhedron around the central Sm^{III} ion is a distorted dodecahedra. Each 4-carboxylate group of $Hpimda^{2-}$ ligand connects two adjacent Sm^{III} atoms to form a dimer in an anti-anti chelating mode and the oxalate assembles these dimers into a corrugated-shape 1D chain approximately along the crystallographic *b* axis. These chains are further connected into a spectacular 2D grid with repeating Sm6 unit by the 5-carboxylate group of the $Hpimda^{2-}$ ligand (Fig. 19a). Two adjacent 2D sheets with the hexagonal Sm_6 SBUs (Fig. 19b) are further linked by oxalate resulting in a 3D framework structure (Fig. 19c). In case of Tb^{III} (Fig. 19d), Dy^{III} and Ho^{III} compounds, temperature-dependent magnetic susceptibility studies suggest ferromagnetic couplings between adjacent magnetic centres bridged through oxalate s. However, the observed magnetic data is quite different for the Er^{III} compound (Fig. 19e) and the feature was attributed to possible

consequence of intramolecular antiferromagnetic interactions and the thermal depopulation of the Er^{III} excited states (Stark sublevels of the $^2H_{11/2}$, $^4I_{13/2}$, and $^4S_{3/2}$ states).

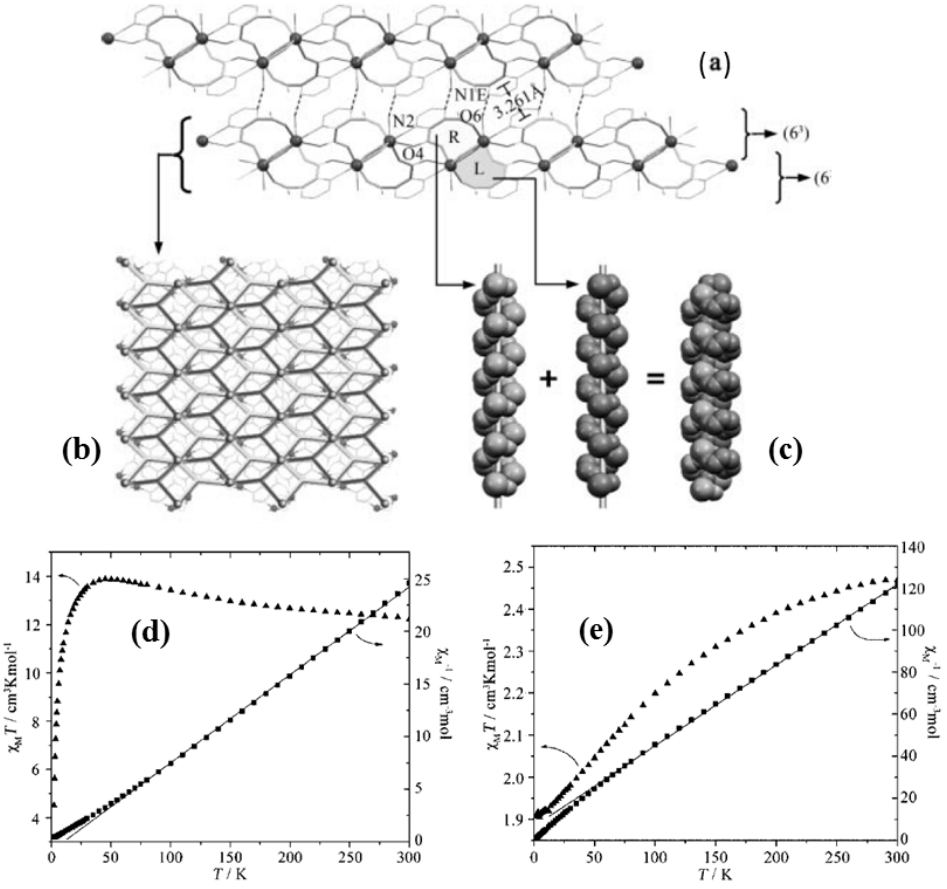

Fig. 18. (a) 2D crystal packing diagram along the crystallographic *b* axis for $[Y(pza)(OH)(H_2O)]_n$ (**1**) showing interlayer interactions where H- bonds are indicated by dashed lines and π–π interactions by arrows and helical chains. (b) Topological representation of along crystallographic *c* axis. (c) Space-filling diagram showing that the helices are founded from two homochiral chains. (d) Plots of the temperature dependences of χ_M^{-1} and $\chi_M T$ for $[Er(pza)(OH)(H_2O)]_n$ (**2**) and (e) for $[Yb(pza)(OH)(H_2O)]_n$ (**3**). Reproduced with permission from reference [31].

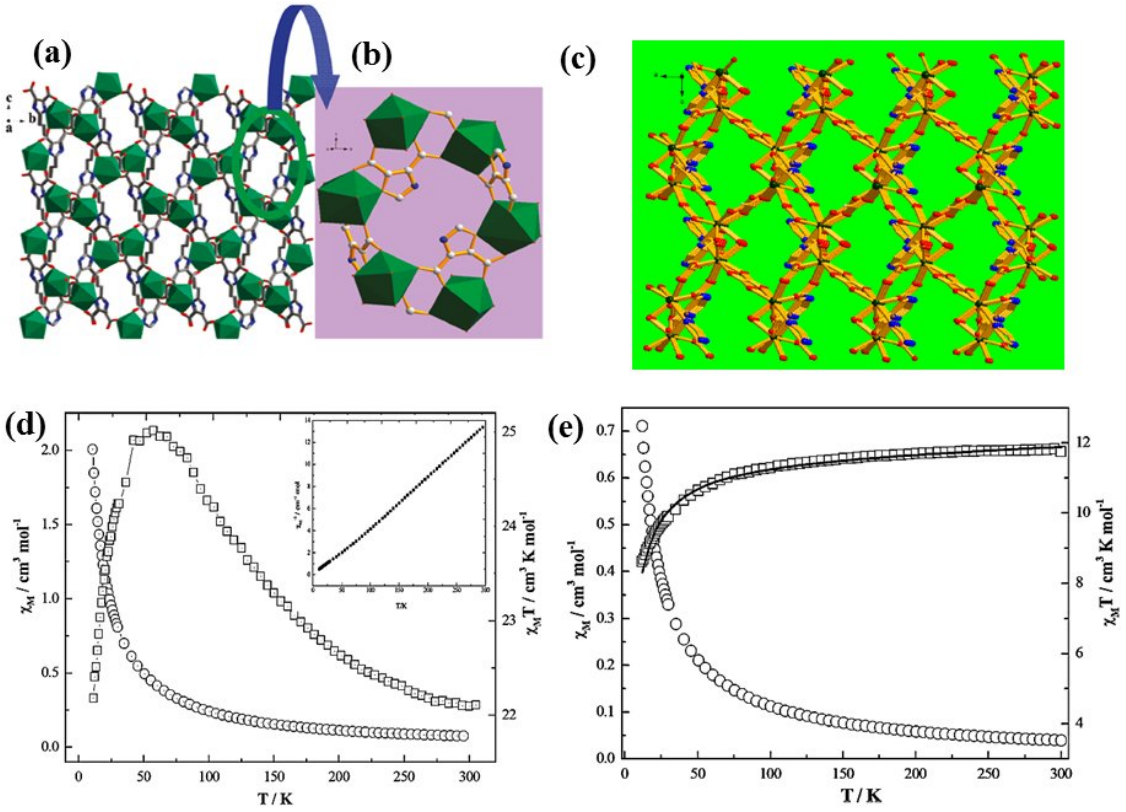

Fig. 19. (a) Polyhedron view of the 2D network of $\{[Sm_2(Hpimda)_2(\mu_4\text{-}C_2O_4)\cdot 2H_2O]\cdot 4H_2O\}_n$ (**1**) down the *a*-axis. (b) An individual Sm_6 hexagonal ring viewed approximately down the *a*-axis. (c) The 3D view of **1**. (d) Plots of $\chi_M T$ and χ_M against temperature *T* for $\{[Tb_2(Hpimda)_2(\mu_4\text{-}C_2O_4)\cdot 2H_2O]\cdot 4H_2O\}_n$ (**3**). The inset shows χ_M^{-1} as the function of temperature. (e) Temperature dependence of $\chi_M T$ and χ_M for $\{[Er_2(Hpimda)_2(\mu_4\text{-}C_2O_4)\cdot 2H_2O]\cdot 4H_2O\}_n$ (**6**). Reproduced with permission from reference [121].

Another report by Manna and co-workers described isomorphous 3D LOFs with the general formula $\{[Ln^{III}_2(suc)_3(H_2O)_2].0.5H_2O\}_n$, suc = succinate dianion, Ln = Pr (**1**), Nd (**2**), Sm (**3**), Eu (**4**), Gd (**5**), and Dy (**6**)] [117]. These compounds have 3D architecture where each Ln ion located in a nine-coordination geometry accomplished by eight oxygen atoms from succinate and one oxygen atom from an aqua ligand. The lanthanide polyhedra and succinates form layers which further assemble by another succinate to construct a 3D framework. There are two crystallographic independent dicarboxylates are involved in the architecture assembly. The corrugated layers lie in the crystallographic *ab* plane with lanthanide ions connected by succinate ligands (Fig. 20a) and along crystallographic *c* axis the layers are

connected by centrosymmetric succinate fragments (Fig. 20b). Ferromagnetic interaction is observed in case of Gd^{III} and Dy^{III} compounds, while Pr^{III} (**1**), Nd^{III} (**2**), Sm^{III} (**3**) and Eu^{III} (**4**) compounds show antiferromagnetic interaction. The magnetic behaviour of the Gd^{III} and Dy^{III} compounds are shown in Fig. 20c and 20d, respectively. To understand the magnetic behaviour, density functional calculation supports the ferromagnetic interaction between Gd^{III} ions in **5** and classical crystal field approach was adopted for the rest of the compounds. The reason for the observed ferromagnetic interaction in Dy^{III} analogue was not clear. Indeed, the complex interactions in Ln ions still need detail insight and more exploration of new compounds.

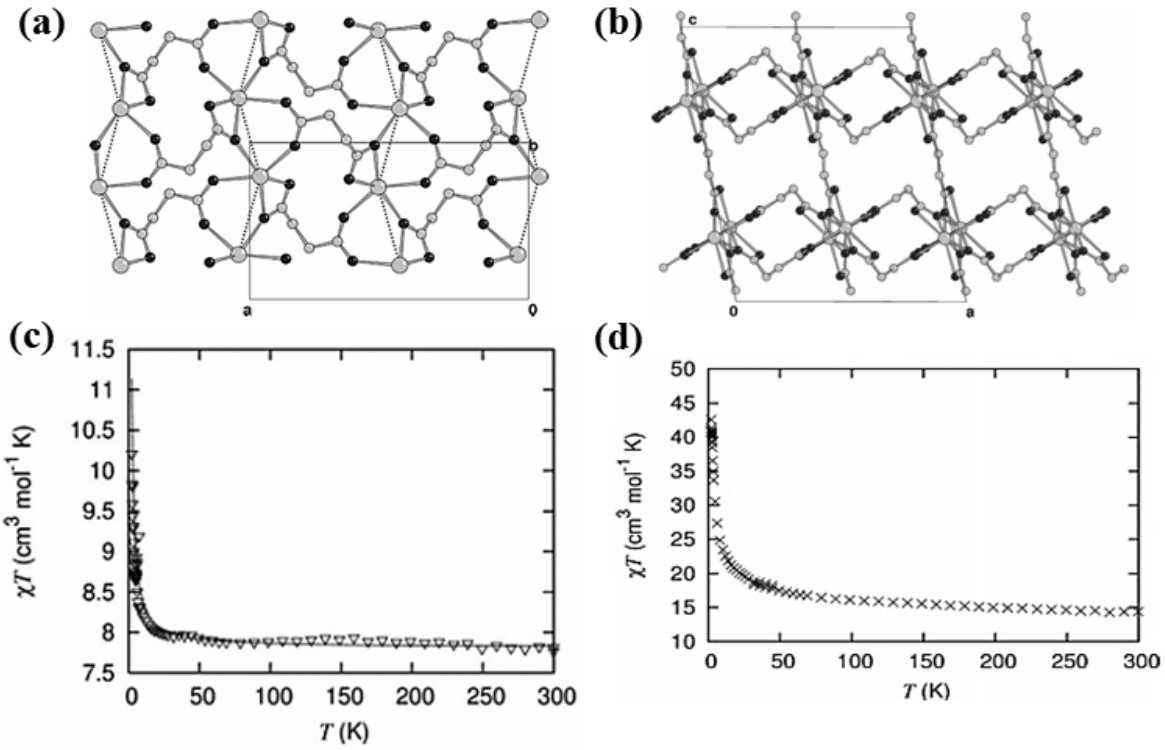

Fig. 20. (a) Corrugated layers in the crystallographic *ab* plane. (b) Crystal packing showing layers connected by centrosymmetric succinate fragments along axis *c*. (c) Temperature dependence of the magnetic susceptibility of $\{[Gd^{III}_2(suc)_3(H_2O)_2].0.5H_2O\}_n$ (**5**). (d) Temperature dependence of the magnetic susceptibility of $\{[Dy^{III}_2(suc)_3(H_2O)_2].0.5H_2O\}_n$ (**6**). Reproduced with permission from reference [117].

It should be noted that the magnetic interaction in lanthanides are often weak due to trivial interaction of the diffused orbitals. Although there is no particular guide to strengthen the coupling, some judicious synthetic strategy has been conceived to overcome such inconvenience. One example is connection of paramagnetic metal ions by polytopic

organic radicals as they can act as magnetic relay. Moreover, the appropriate polytopic radical system can also usher porosity, thus eventually resulting multifunctional magneto-porous system. Datcu and co-worker have reported such lanthanide–radical frameworks based on PTM radicals [PTM = perchlorinated triphenylmethyl (trityl)] [122]. Frameworks based on the PTMTC radical (tricarboxylate of PTM) as well as the non-magnetic counterpart of the radical (αH-PTMTC) were fabricated and they are {[Ln(PTMTC)$(EtOH)_2H_2O$]·xH_2O, yEtOH}$_n$ [Ln=Tb (**1**), Gd (**2**), Eu (**3**)] and {[Ln(αH-PTMTC)$(EtOH)_2H_2O$]·xH_2O, yEtOH}$_n$ [Ln=Tb (**1'**), Gd (**2'**), Eu (**3'**)]. Compound **1-3** and **1'-3'** are isomorphous and single-crystal structure determination revealed neutral 3D framework assembled from paddlewheel M^{III}-carboxylate dimers, which are bridged by tricarboxylate PTMTC ligands in a *syn-syn* fashion. The PTMTC ligands locate themselves with a trigonal geometry where three carboxylate groups are present in *para* position to the central carbon atom and act as three-connected nodes. The paddle-wheel units are surrounded by six bridging PTMTC radicals and the dimeric units can be represented as six-connected nodes; thus resulting unique (6,3)-connected 3D framework. The framework contains helical channels propagating along crystallographic *b* axis (Fig. 21a).The temperature dependent magnetic susceptibilities for **1-3** are presented in Fig. 21b. For the Tb^{III} compound (**1**), the low-temperature magnetic behaviour was attributed to the depopulation of the Stark sublevels associated to the crystal field effects, {Ln–Ln} and {Ln–radical} magnetic interactions. For Gd^{III} compound (**2**), the absence of orbital contribution suggests that in this case, the magnetic signature is due to {Ln–Ln} and {Ln–radical} magnetic interactions. The ground state of Eu^{III} is non-magnetic and hence the monotonous decrease in χT value for the Eu^{III} compound (**3**) was ascribed to the depopulation of the thermally excited energy levels, which are close enough to the ground state to be thermally populated at room temperature. In addition, the radical-radical interaction was also accounted for the observed antiferromagnetic interaction. Since **1**–**3** and **1'-3'** are isostructural and the ligand field effect is the same irrespective of the ligand PTMTC or αH-PTMTC, thus the Stark sublevels for the corresponding coordination polymers will give identical energy spectra. Hence, the magnetic properties of compounds **1'-3'** should correspond to the intrinsic ion contributions of the Ln^{III} ions and were used to reveal the exchange interactions in **1–3**. The magnetic properties of **1'-3'**were studied and the χ(x')T products were mathematically subtracted from the $\chi(x)T$ ones [x=**1-3**; x'=**1'-3'**] to give $\Delta\chi^{Ln}T=\chi(x)T - \chi(x')T$ for each Ln^{III} ion. The low temperature profile of $\Delta\chi^{Ln}T$ plot shows decrease of the $\Delta\chi^{Ln}T$ value for Eu^{III} compound; while an increase is observed for Tb^{III} and

Gd^{III} compounds (Fig. 21c, 21d). These magnetic signatures were ascribed to the antiferromagnetic {radical-radical} interaction for Eu^{III} compound (since the ground state is non-magnetic) and ferromagnetic {Ln-radical} interaction in Tb^{III} and Gd^{III} compounds. However, for **2**, the χT behaviour at low temperature suggested antiferromagnetic behaviour and similar decrease was also observed in **2'**(Fig. 21d). This observation was attributed to the {Gd– Gd} exchange coupling through carboxylate. Thus for **2**, the magnetic behavior at low temperature was a cumulative effect of the concomitant contributions of both {Gd–Gd} and {Gd–radical} interactions and the latter was revealed by $\Delta\chi^{Gd}T$ vs T plot.

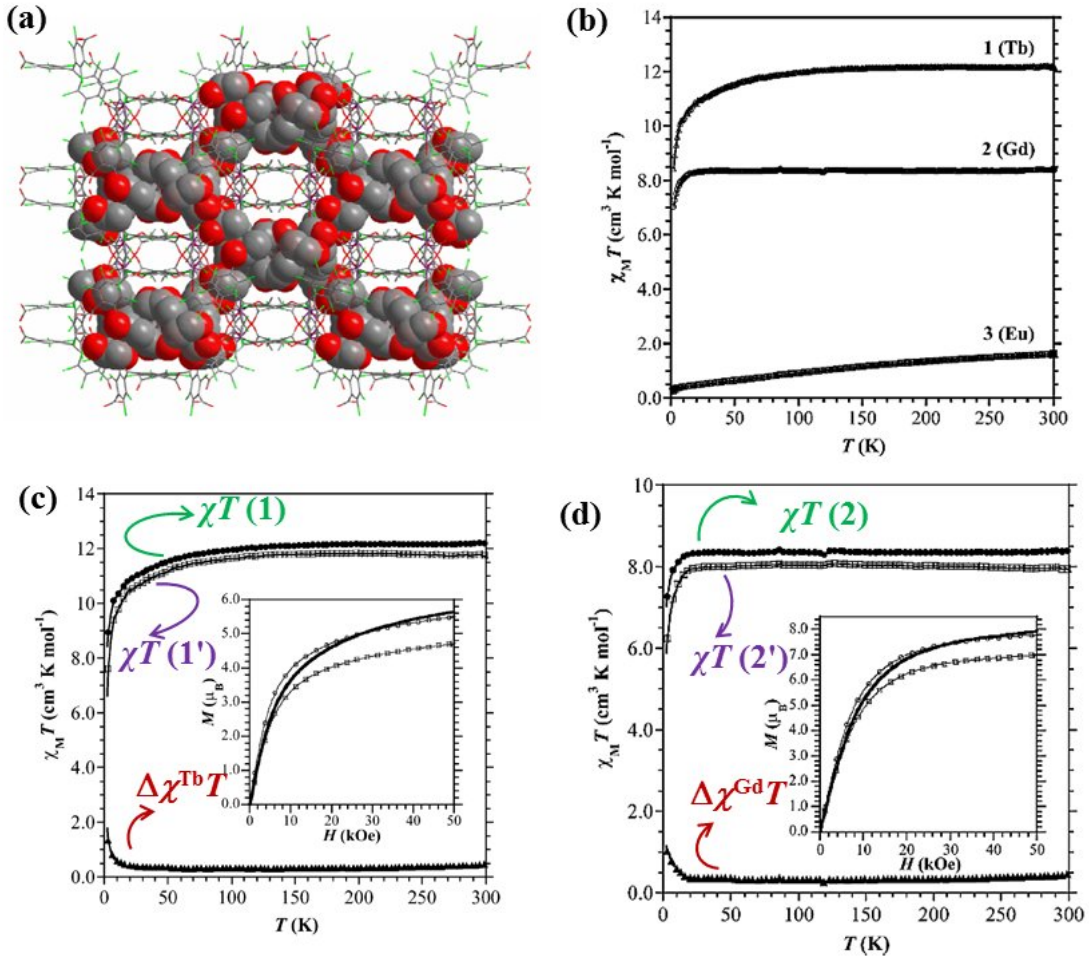

Fig. 21. (a) View of the 3D framework of **1** containing the disordered guest solvent molecules (space filling representation) in the channels. (b) Plots of $\chi_M T$ against T for **1-3**. (c) Temperature dependence of $\chi_M T$ of **1**, **1'** and $\Delta\chi^{Tb}T$ in Tb^{III}-based compounds **1** and **1'**. (d) Temperature dependence of $\chi_M T$ of **2**, **2'** and $\Delta\chi^{Gd}T$ in Gd^{III}-based compounds **2** and **2'**. Reproduced with permission from reference [122].

4.2 *Slow relaxation of magnetization in Ln-organic frameworks*

The slow magnetic relaxation behaviour is one important feature of anisotropic compounds and exploration of such relaxation properties of molecular materials has attained considerable research interests to the chemists and materials scientists. In this regard, synthesis and study of the SMMs and single-chain magnets SCMs have attracted considerable research interests [104-115]. In 1991, Gatteshchi and co-workers first discovered SMM property in the celebrated "Mn_{12}" cluster [105, 106], which was structurally characterized by Lis [107]. Thereafter, this field had witnessed a rapid growth. The detail discussion of SMMs based in lanthanide clusters and heterometallic lanthanide-transition clusters is beyond the scope of this review and we will discuss here about the slow relaxation behaviour of 3D LOFs only. In 3D frameworks too, such behaviour could be observed due to the single-ion anisotropy of the metal ion. Although relaxations in 3D compounds have not been studied to the extent of those zero-dimensional compounds (SMMs), a handful of reports are available [30, 123]. We will present here an illustrative example of slow relaxation for 3D framework compound. Song *et al.* [123] have reported ferromagnetic interaction and slow magnetic relaxation in purely Ln based frameworks. In their contribution, they have reported two lanthanide-organic frameworks, $\{Ln(TDA)_{1.5}(H_2O)_2\}_n$ [Ln = Gd (**1**), Dy (**2**)]. These two frameworks are isomorphous and the Ln ions adopt distorted bicapped trigonal prism geometry. In **1**, three adjacent Gd^{III} ions are bridged by the carboxylic groups of TDA ligands to furnish a triangular $\{Gd_3\}$ motif with approximately identical edges. These triangular units further assemble through the carboxylic groups to generate 1D belt-like chain along the crystallographic *b* direction (Fig. 22a). The TDA ligand is present in two different types of coordination modes in the framework structure. The adjacent 1D chains are linked by these different coordination modes of TDA to furnish the 3D structure (Fig. 22b). Both these compounds exhibit ferromagnetic interaction between the Ln ions, as evident from their temperature dependent $\chi_M T$ profile (Fig. 22c, 22d). Additionally, slow magnetic relaxation behaviour has been observed for **2** (Fig. 22e). Frequency dependent behaviours have been observed for both the real and imaginary part of susceptibility below 7 K. The energy barrier was calculated using Arrhenius law and the best fitting yielded an energy barrier of 44.2 K with relaxation time 2.4×10^{-8} s.

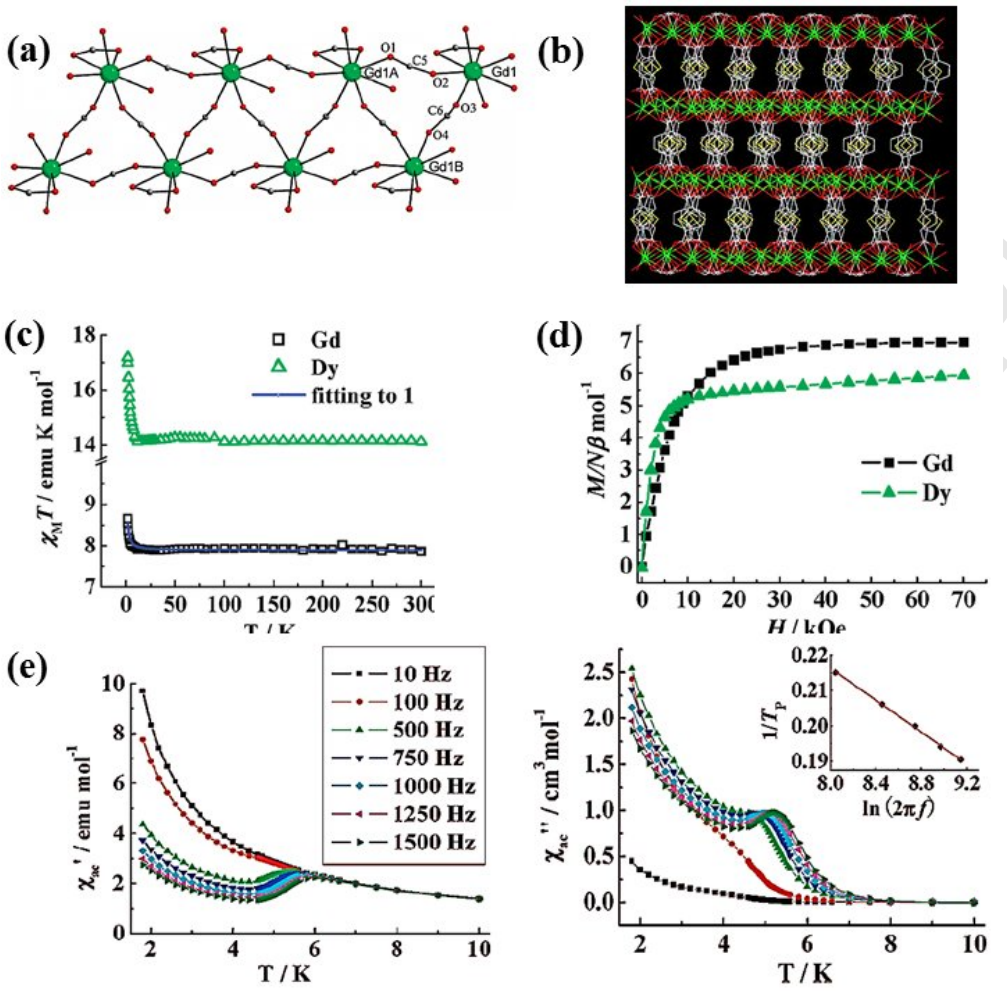

Fig. 22. (a) The 1D beltlike chain of $\{Ln(TDA)_{1.5}(H_2O)_2\}_n$ constructed by the triangular $\{Gd_3\}$ motif along the crystallographic *b* direction. Colour codes: green, Gd; red, O; gray, C. Other atoms were omitted for clarity. (b) The 3D framework fabricated by connection of adjacent 1D belt-like chains through TDA bridging ligands. (c) Plots of temperature dependent $\chi_M T$ profile of $\{Gd(TDA)_{1.5}(H_2O)_2\}_n$ (**1**) and $\{Dy(TDA)_{1.5}(H_2O)_2\}_n$ (**2**) (d) Field dependence of magnetization of compounds **1** and **2** at 1.8 K. (e) ac magnetic measurements for **2** at H_{ac} = 3 Oe and H_{dc} = 0. Inset: Solid line representing the least-squares fit of the experimental data to the Arrhenius equation for **2**. Reproduced with permission from reference [123].

5. Dual magneto luminescent system and guest induced change in magnetic behaviour

As we have discussed earlier, LOFs have already established themselves as highly promising materials ushering new magnetic and luminescent compounds. A recent trend is to furnish bi-functional materials combining magnetic and luminescent properties. Huang *et al*.

reported weak ferromagnetic interactions and typical luminescence properties of Tb^{III} ion in the visible region in a Tb^{III}- based 3D framework $[Tb_2(tdc)_3(H_2O)_4]_n$ [124]. Harbuzaru *et al.* also reported a Tb^{III} framework that showed anisotropic photoluminescence behaviour and ferromagnetic Tb^{III}–Tb^{III} interaction [98]. The magnetic properties of the series of frameworks $[Ln(pza)(OH)(H_2O)]_n$ [Ln = Y (**1**), Er (**2**), Yb (**3**)] reported by Weng *et al.* [30] had already been discussed previously. These frameworks are also representative of bi-functional magento-luminiscent materials. The upconversion luminescence properties were studied for the co-doped lanthanide (Y: Er, Yb) coordination compounds.

Other than exploiting the homometallic LOFs, an approach to fabricate such dual frameworks is the employment of heterometallic chemistry, where a combination of lanthanide and transition metal ions are frequently used. Such compounds are synthesized by self-assembly of d-f metal ions with polydentate ligand having O and N atoms (such as pyrazine dicarboxylic acid, pyridine dicarboxylic acid, imidazole dicarboxylic acid etc [125]. This approach relies on the fact that the hard Ln^{III} ions have affinity for hard O donors while the transition metals ions favour coordination to the soft N donors. In this regard, 3d-4f and 4d-4f compounds are noteworthy. Zhao *et al.* reported a honeycomb type 2D compound with the formula $\{[Dy(hpd)_3Mn_{1.5}(H_2O)_3].3.125H_2O\}_n$ (hpd = 4-hydroxylpyridine-2,6-dicarboxylic acid [126]. This compound shows ferromagnetic coupling between Mn^{II} and Dy^{III} ions. The emission of this compound in DMF increases considerably in the presence of Mg^{II} ions, thereby making the compound useful for sensory purposes. This enhanced emission has been attributed to the coordination of Mg^{II} ions to the –OH oxygen atoms of the three hpd^{2-} ligands which results in a change in the energy levels of the excited state of the ligands. Eventually, the energy of these excited energy levels matches with those of the Ln, thereby decreasing the non-radiative energy loss which originates from thermal vibration of O-H groups. It is noteworthy that most of the literature reports discussed only about multifunctional materials, while for designing practical devices the goal would be to furnish switchable materials with tuneable properties. Thus it would be more interesting if the compound exhibiting different properties can be a real magneto-optic switching compound.

We have discussed only non-porous compounds so far. Indeed, the properties become much more interesting with the introduction of porosity in luminescent and magnetic LOFs. Furnishing porous and magnetic frameworks remains always difficult because of the incompatibility in the properties. In general, the strength of magnetic coupling decreases with distance while porosity is usually enhanced with the large separation between the metal nodes. Thus, synthesis of a microporous solid that behaves as a magnet remains an open

challenge. In this regard, we have previously mentioned the strategy of by Dactu *et al.* [122] where they have reported the linkage of magnetically active metal ions by persistent polytopic organic radicals to strengthen the magnetic interaction; although the porous properties were not studied in detail in this report.

The guest molecules could be exploited to control the magnetic properties of the compounds and there are few elegant systems showing such fascinating behaviour [127, 128]. In this regard, Ln-based systems are yet to be explored properly as they can serve as promising guest responsive magnetic and luminescent materials. Furthermore, there is an additional opportunity to observe slow relaxation of magnetization, which would arise from the typical anisotropic behaviour of the lanthanides. Our group has reported an interesting case of solvent responsive bimodal magnetic and luminescence properties in a multifunctional bimetallic Dy^{III}-K^{I} oxalate framework, $\{KDy(C_2O_4)_2(H_2O)_4\}_n$ (**1**) ($C_2O_4^{2-}$ = oxalate dianion) (Scheme 2) [129]. In this work, the choice of the central metal ion is very crucial. We have exploited Dy^{III} ions by using the appropriate ligand system because of high spin and large magnetic anisotropy. In addition, luminescence property of Dy^{III} has culminated in metal based emission in the visible region.

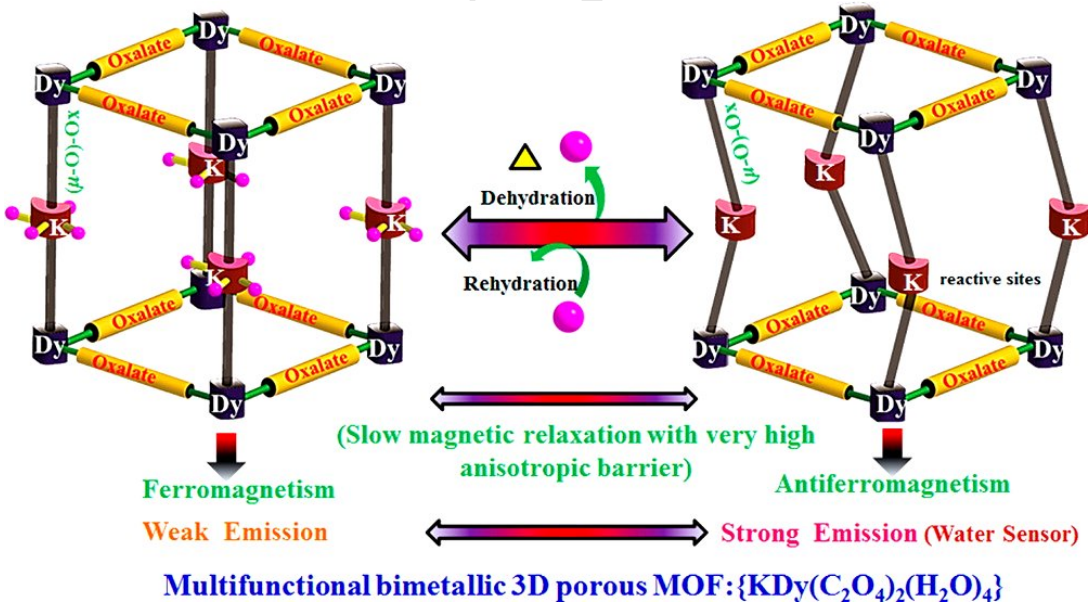

Scheme 2. Solvent induced structural change and corresponding magnetic and luminescent Properties in $\{KDy(C_2O_4)_2(H_2O)_4\}_n$ (**1**) . Reproduced with permission from reference [129].

1 is a neutral 3D bimetallic coordination framework of Dy^{III} and K^{I} bridged by the oxalate linkers (ox^{2-}) (Fig. 23). Here the magnetically innocent K^{I} ion is an integral part of the framework and acts as a potentate of the structure. Each octacoordinated Dy^{III} centre

locate itself in a distorted square-antiprismatic coordination geometry and chelated to four different ox^{2-} through the oxygen atoms (O1 and O2) and each octacoordinated K^I centre are connected to four oxygen atom (μ_2-O1) of ox^{2-} and rest of the four coordination numbers were satisfied with four H_2O molecules (O1w) (Fig. 23a). After removal of the K^I bound H_2O molecules the 3D framework may generate bidirectional channels with the dimensions of 3.5 × 3.5 $Å^2$ along the *c*-axis and 2.0 × 1.1 $Å^2$ along other direction (perpendicular to *a* axis) (Fig. 23c and 23d). Compound **1** undergoes reversible structural change. Thermal stability and structural reversibility was investigated through TGA and PXRD analysis. TGA suggests that four H_2O molecules bound to K^I site are released in the temperature range of 45−120 °C and the dehydrated solid (**1′**) is stable up to 380 °C. PXRD pattern of **1′** shows sharp lines with shifting of few peak positions, and appearance of some new peaks compared to **1**, suggesting structural transformation to lower symmetry after loss of K^I bound H_2O molecules. After exposing **1′** to water vapour for three days, the as-synthesized framework was again regenerated, which was confirmed by PXRD pattern.

The dehydrated compound **1'** adsorbs H_2O (kinetic diameter 2.8 Å), MeCN (4.3 Å) and MeOH (4.0 Å) in two steps but the occlusion of EtOH (4.5 Å) occurs in one step (Fig. 24). The H_2O vapour sorption profile exhibits rapid uptake at low pressure region and incomplete desorption suggesting strong interaction with the pore surfaces and it has been correlated to the presence of unsaturated K^I site.

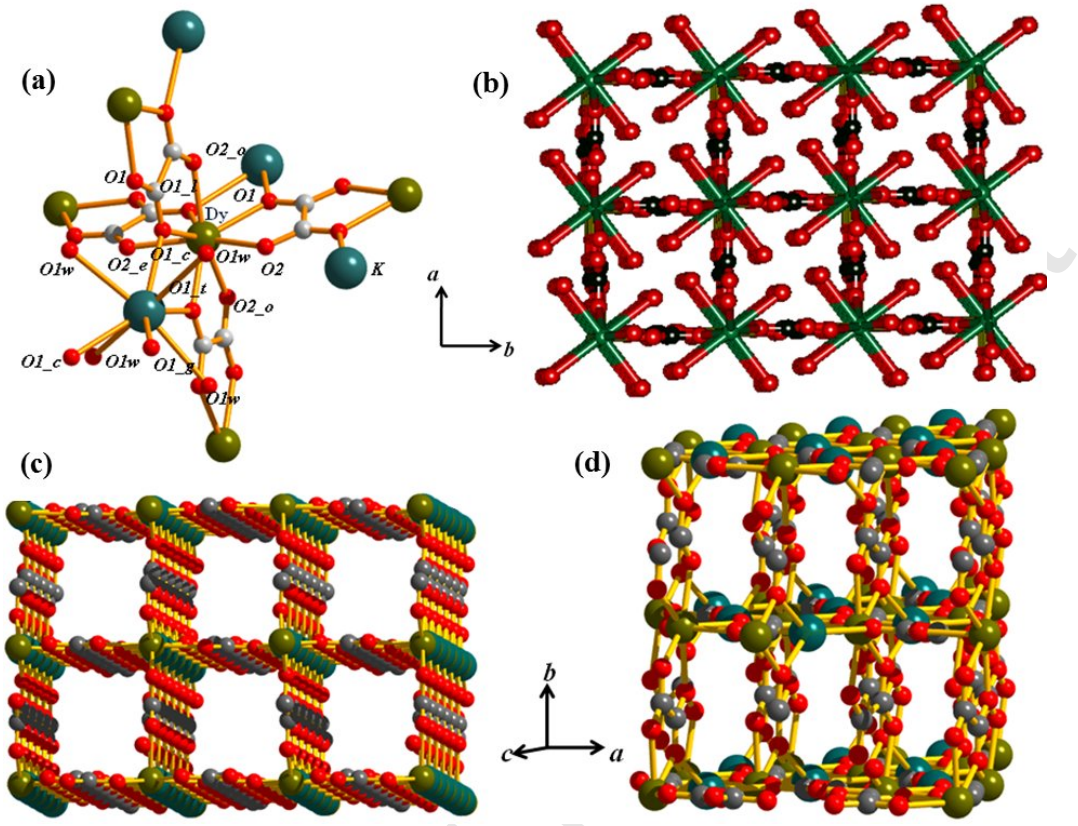

Fig. 23. (a) The coordination environment of Dy^{III} and K^{I} in $\{KDy(C_2O_4)_2(H_2O)_4\}_n$ (**1**). (b) Extended 3D structure of **1** built by the ox^{2-} linker bridging Dy^{III} and K^{I} alternatively along the crystallographic *c* axis. (c) View of the 1D channels after removing H_2O molecules along the crystallographic *c* axis. (d) The small channels viewed perpendicular to crystallographic *b* axis. Reproduced with permission from reference [129].

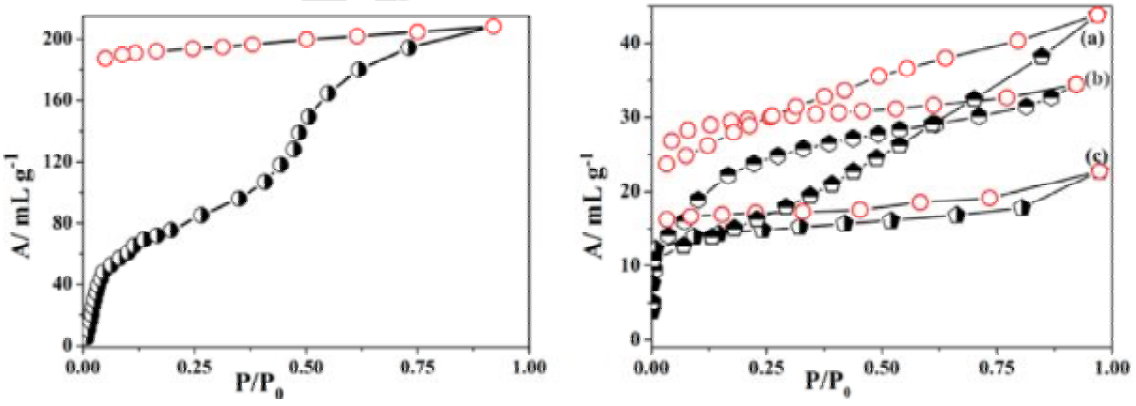

Fig. 24. Solvent sorption isotherms for **1′**: (left) H_2O at 298 K, (right) (a) MeCN at 298 K (b) MeOH at 293 K, and (c) EtOH at 298 K. P_0 is the saturated vapour pressure of the respective solvent at the mentioned temperature. Reproduced with permission from reference [129].

The most exciting characteristic of **1** is its magnetic properties. The plots of χ_M and $\chi_M T$ of **1** evidenced presence of weak ferromagnetic interaction between the Dy^{III} centres (Fig. 25a). The linear fitting of χ_M^{-1} of **1** at 290-40 K deduce the Weiss constant (θ) = 11.3 K which supports the presence of ferromagnetic interaction. This ferromagnetic interaction in **1** get interrupted through dilution effect, which was investigated through the synthesis and study of another isostructural framework $\{KDy_{0.25}Y_{0.75}(C_2O_4)_2(H_2O)_4\}_n$ (**2**) containing a 3:1 ratio of Y^{III} and Dy^{III}. The magnetic measurement of **2** showed that it is magnetically different from **1** and the ferromagnetic interaction was not operating unlike **1**, which was attributed to the longer Dy---Dy distance in **2**. The dehydrated compound **1'** showed antiferromagnetic interaction operating in the system. Curie-Weiss fitting of χ_M^{-1} vs T plot for **1'** over the whole temperature range deduced Weiss constant (θ) of -3.88 K. We speculated that this ferromagnetic to antiferromagnetic phase transition after dehydration is a consequence of structural change leading to the change in magnetic interaction. For the rehydrated framework, the $\chi_M T$ value gradually increases from 300 K upon decreasing the temperature and reaches maximum at 50 K and again decreases on further cooling due to the depopulation of excited state Starks level (Fig. 25a). The Curie-Weiss fitting of χ_M^{-1} vs T in the range 290−40 K deduced positive θ value of 3.65 K, advising reappearance of ferromagnetic interaction and the smaller θ value compared to the as-synthesized compound (**1**) suggested that the rehydration was incomplete. The alternating current (ac) magnetic measurement shows that both the real $\chi_M' T$ and imaginary χ_M'' part of the ac susceptibilities shows strong frequency dependence below 53 K (Fig. 25c). The calculated energy barrier ($\Delta E/K_B$) and relaxation time (τ_0) using Arrhenius law are = 417 ± 9 K and 1.23×10^{-09} S, respectively. Dehydrated compound **1'** also shows similar frequency dependence with $\Delta E/K_B$, τ_0 values of 418± 7 K and 3.0×10^{-09} S respectively, which are very close to that for the as-synthesized compound **1**. Thus the dynamics of the magnetization is independent of the nature of magnetic interaction between two neighbouring Dy^{III} centres and the sole factor resulting this slow magnetic relaxation is the single-ion magnetic anisotropy. **1** also showed interesting luminescence behaviour. The luminescent spectrum of **1** exhibits two characteristics peaks of Dy^{III} at 485 nm and 576 nm, which corresponds to $^4F_{9/2} \rightarrow {}^6H_{15/2}$, $^4F_{9/2} \rightarrow {}^6H_{13/2}$ transitions, respectively. In the dehydrated compound (**1'**), the intensities of both these characteristic emission peaks were enhanced and slightly blue shifted compared to as-synthesized compound **1**. H_2O molecules exhibit strongest quenching effect compared to other solvents MeOH, MeCN and EtOH, evoking **1′** as a potential H_2O sensor.

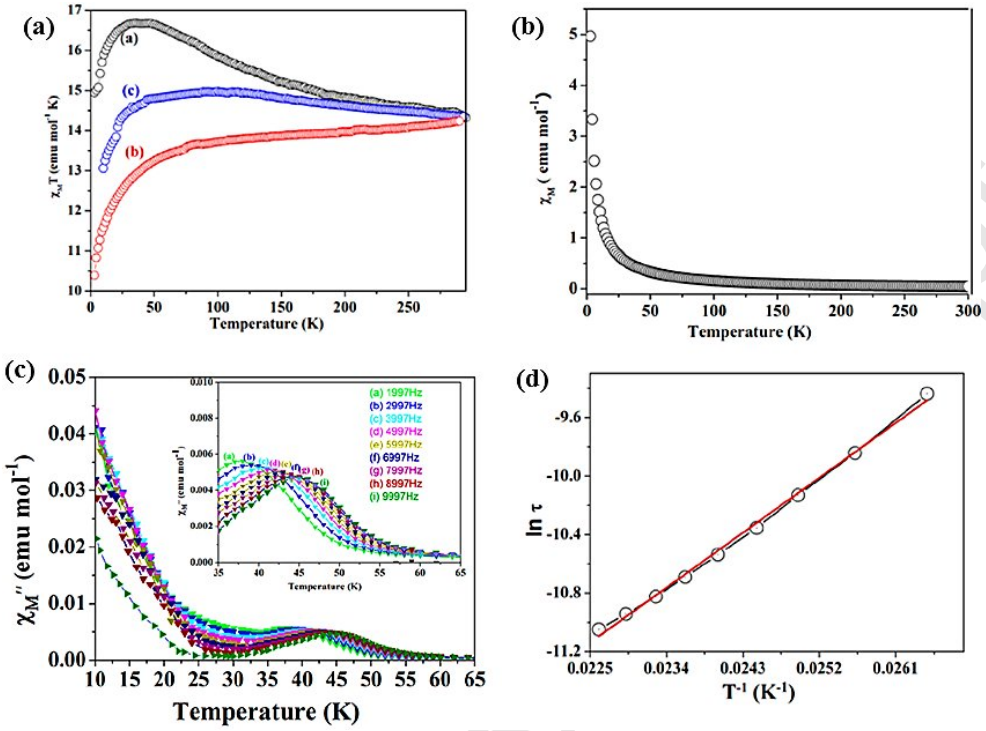

Fig. 25. (a) Plot of the $\chi_M T$ as a function of temperature for as-synthesized $\{KDy(C_2O_4)_2(H_2O)_4\}_n$ (**1**) (black), dehydrated (**1′**) (red) and rehydrated (**1″**) (blue) compound. (b) χ_M as a function of temperature for **1**.(c) Frequency dependence of the imaginary χ_M'' part of **1**. (d) Linear fitting of the frequency dependence of χ_M'' by Arrhenius law. The solid red line represents the least-squares fitting of the experimental data. Reproduced by permission from reference [129].

This work showed that LOFs are promising materials and they can usher new concepts to fabricate new smart materials which combine porosity, extraordinary anisotropic barrier, solvent induced modulation in magnetic and luminescent properties.

6. Conclusion and outlook

The number of reports involving lanthanide-organic frameworks is increasing with time ever since the hurdles in their synthesis of stable compounds and proper structural characterization have been overcome. Design and synthesis of highly thermally stable and permanently porous lanthanide frameworks are feasible and recent few reports have demonstrated potential of these framework materials for H_2 storage and CO_2 capture applications. Therefore new lanthanide framework materials for CO_2 capture and H_2 storage applications can be envisioned by incorporating open metal sites within the framework along with the suitable design of the organic linkers. Furthermore fabricating heterometallic

frameworks with lanthanide and alkali metal cations offer a viable strategy to such applications. The ease of incorporating different donor-acceptor lanthanide ion pairs within the same framework can give rise to effective colour tunablity. Nanoscale synthesis of such frameworks will also offer solution processability and enhance their practical applicability. Also the incorporation of ligands containing –OH groups to form luminescent lanthanide frameworks will generate a material for effective sensing of selective metal ions based on their coordinating properties.

As discussed, lanthanide frameworks would serve as potential molecular magnetic materials. Although the exact depiction of such systems remains difficult owing to the complex magnetic behaviour, many excellent reports have been documented showing the interesting behaviour and the promise of such materials. The large single-ion anisotropy and slow relaxation of magnetization are important aspects of the lanthanide systems and these properties are promising to usher new devices. However, there is indeed a dearth of proper understanding of magnetic behaviour of lanthanides. Chemists and physicists will continue to contribute to furnish novel materials and to investigate these materials to get the insight of the magnetism. Finally, developing multifunctional compounds is the ultimate goal of the material scientists. The future smart materials must contain different properties like luminescence, porosity and magnetism; which could be combined. It should be mentioned that many reports have documented such bifunctional (having porosity and magnetism, or luminescence and magnetism) and even multifunctional lanthanide frameworks, but real sensory materials with mutual dependence of the different properties and switchable properties are yet to be explored. Guest dependent magnetism is also rarely accounted in lanthanides frameworks. Hence the future goal will be to generate such multifunctional devices exploiting lanthanide compounds using a very judicious synthetic design strategy.

List of Abbreviations

PCP Porous Coordination Polymers

MOF Metal Organic Frameworks

LOF Lanthanide Organic Frameworks

UMS Unsaturated Metal Sites

BDC 1,4-benzene dicarboxylate

BPDC 4,4'-dicarboxylate-2,2'-dipyridine

CCS Carbon Capture and Sequestration

DMF N,N- dimethyl formamide

MIL Material of Institut Lavoisier

PDC pyridine-3,5-dicarboxylate

BTC 1,3,5-benzenetricarboxylate

DFT Density Functional Theory

H_2FTZB 2-fluoro-4-(1H-tetrazol-5-yl)benzoic acid

MBB Molecular Building Block

PDA 1,4-phenylendiacetate

SBU Secondary Building Unit

imidc 4,5-imidazoledicarboxylic acid

dhbdc 2,5-dihydroxyterephthalate

H_3L 4,4′,4″-(benzenetricarbonyltris-(azanediyl))tribenzoic acid

Mu^{2-} Mucicate

BTB 4,4',4"-benzene-1,3,5-triyl-tri-benzonate

ICP infinite coordination polymer

3-TPyMNTB tris((pyridin- 3-ylmethyl)benzoimidazol-2-ylmethyl)amine

L 1,4,8,-11-tetraazacyclotetradecane-1,4,8,11-tetrapropionic acid

G Guest solvent

pzdc 2,5-pyrazinedicarboxylate

H_2ox oxalic acid

TATB triazine-1,3,5-tribenzoate

DMA N,N-dimethylacetamide

SMM Single Molecule Magnet

SCM Single Chain Magnet

pza 2,3-pyrazinedicarboxylate

H_3pimda 2-Propyl-1H-imidazole-4,5-dicarboxylic acid

suc succinate dianion

PTM perchlorinated triphenylmethyl (trityl)

TDA thiophene-2,5-dicarboxylic acid

tdc deprotonated thiophene 2,5-dicarboxylic acid

hpd 4-hydroxylpyridine-2,6-dicarboxylic acid

References:

[1] Q. Yue, J. Yang, G.-H. Li, G.-D. Li, J.-S. Chen, Inorg. Chem. 45 (2006) 4431.

[2] Y. Liu, K. Mo, Y. Cui, Inorg. Chem. 52 (2013) 10286.

[3] S. Aime, M. Fasano, E. Terreno, Chem. Soc. Rev. 27 (1998) 19.

[4] S. P. Fricker, Chem.Soc.Rev. 35 (2006) 524

[5] M. D. Allendorf, C. A. Bauer, R. K. Bhakta, R. J. T. Houk, Chem. Soc. Rev. 38 (2009) 1330.

[6] N. Sabbatini, M. Guardigli, J.-M. Lehn, Coord. Chem. Rev. 123 (1993) 201.

[7] B. L. Chen, Y. Yang, F. Zapata, G. D. Qian, Y. S. Luo, J. H. Zhang, E. B. Lobkovsky, Inorg. Chem. 45 (2006) 8882.

[8] D. T. de Lill, N. S. Gunning, C. L. Cahill, Inorg. Chem. 44 (2005) 258.

[9] D. T. de Lill, A. de Bettencourt-Dias, C. L. Cahill, Inorg. Chem. 46 (2007) 3960.

[10] Y. K. Park, S. B. Choi, H. Kim, K. Kim, B. H. Won, K. Choi, J. S. Choi, W. S. Ahn, N. Won, S. Kim, D. H. Jung, S. H. Choi, G. H. Kim, S. S. Cha, Y. H. Jhon, J. K. Yang, J. Kim, Angew. Chem., Int. Ed. 46 (2007) 8230.

[11] X. Rao, Q. Huang, X. Yang, Y. Cui, Y. Yang, C. Wu, B. Chen, G. Qian, J. Mater. Chem. 22 (2012) 3210.

[12] K. Liu, H. You, Y. Zheng, G. Jia, Y. Huang, M. Yang, Y. Song, L. Zhang, H. Zhang, Cryst. Growth. Des. 10 (2010) 16.

[13] S-L. Zhong, R. Xu, L-F. Zhang, W-G. Qu, G-Q. Gao, X.-L. Wu, A-W. Xu, J. Mater. Chem. 21 (2011) 16574.

[14] Y. Liu, M. Pan, Q-Y. Yang, L. Fu, K. Li, S-C. Wei, C-Y. Su, Chem. Mater. 24 (2012) 1954.

[15] M. Eddaoudi, J. Kim, N. Rosi, D. Vodak, J. Wachter, M. O'Keeffe, O. M. Yaghi, Science 295 (2002) 469.

[16] S. Kitagawa, R. Kitaura, S.-i. Noro, Angew. Chem. Int. Ed. 43 (2004) 2334.

[17] L J. Murray, M. Dinca, J. R. Long, Chem. Soc. Rev. 38 (2009) 1294.

[18] K. Sumida, D. L. Rogow, J. A. Mason, T. M. McDonald, E. D. Bloch, Z. R. Herm, T-H. Bae, J. R. Long, Chem. Rev. 112 (2012) 724.

[19] J. Y. Lee, O. K. Farha, J. Roberts, K. A. Sheidt, S. B. T. Nguyen, J. T. Hupp, Chem. Soc. Rev. 38, (2009), 1450.

[20] S. Horike, M. Dinca, K. Tamaki, J. R. Long, J. Am. Chem. Soc. 130 (2008) 5854.

[21] S. Hasegawa, S. Horike, R. Matsuda, S. Furukawa, K. Mochizuki, Y. Kinoshita, S. Kitagawa, J. Am. Chem. Soc. 129 (2007) 2607.

[22] H. K. Chae, M. Eddaoudi, J. Kim, S. I. Hauck, J. F. Hartwig, M. O'Keeffe, O. M. Yaghi, J. Am. Chem. Soc. 123 (2001) 11482.

[23] P. Kanoo, K. L. Gurunatha, T. K. Maji, J. Mater. Chem. 20 (2010) 1322.

[24] Y. Cui, Y. Yue, G. Qian, B. Chen, Chem.Rev. 112 (2012) 1126.

[25] P. Horcajada, C. Serre, M. Vallet-Regi, M. Sebban, F. Taulelle, G. Férey, Angew Chem., Int. Ed. 45 (2006) 5974.

[26] P. Horcajada, C. Serre, G. Maurin, N. A. Ramsahye, F. Balas, M. Vallet-Regi, M. Sebban, F. Taulelle, G. Férey, J. Am. Chem. Soc. 130 (2008) 6774.

[27] S. Mohapatra, K. P. S. S. Hembram, U. Waghmare, T. K. Maji, Chem. Mater. 21 (2009) 5406.

[28] T. M. Reineke, M. Eddaoudi, M. Fehr, D. Kelley, O. M. Yaghi, J. Am. Chem. Soc. 121 (1999) 1651.

[29] Z. Chen, B. Zhao, P. Cheng, X.-Q. Zhao, W. Shi, Y. Song, Inorg. Chem. 48 (2009) 3493.

[30] M. Fang, J.-J. Li, P.-F. Shi, B. Zhao, P. Cheng, Dalton Trans. 42 (2013) 6553.

[31] D. Weng, X. Zheng, X. Chen, L. Li, L. Jin, Eur. J. Inorg. Chem. (2007) 3410.

[32] D.-L. Long, A. J. Blake, N. R. Champness, C. Wilson, M. Schröder, Angew. Chem. Int. Ed.40 (2001) 2444.

[33] R. K. Pachauri, A Reisinger, IPCC Fourth Assessment Report, Intergovernmental Panel on Climate Change, (2007)

[34] A. W. C. van den Berg, C. Otero Areàn, Chem. Commun. (2008) 668.

[35] B. Wang, A. P. Cote, H. Furukawa, M. O'Keeffe, O. M. Yaghi, Nature. 453 **(**2008) 207.

[36] T. Wu, J. Zhang, C. Zhou, L. Wang, X. Bu, P. Feng, J. Am. Chem. Soc. 131 **(**2009) 6111.

[37] M. P. Suh, H. J. Park, T. K. Prasad, D-W. Lim, Chem. Rev. 112 (2012) 782.

[38] N. L. Rosi, J. Kim, M. Eddaoudi, B. Chen, M. O'Keeffe, O. M. Yaghi, J. Am. Chem. Soc. 127 (2005) 1504.

[39] X-S. Wang, S. Ma, P. M. Forster, D. Yuan, J. Eckert, J.J. Lopez, B. J. Murphy, J. B. Parise, H.-C. Zhou, Angew. Chem. Int. Ed. 47 (2008) 7263.

[40] V. Kiritsis, A. Michaelides, S. Skoulika, S. Golhen, L. Ouahab, Inorg. Chem. 37 (1998) 3407.

[41] T. M. Reineke, M. Eddaoudi, M. OKeeffe, O. M. Yaghi, Angew. Chem. Int. Ed. 38 (1999) 2590.

[42] C. Serre, G. Férey, J. Mater. Chem. 12 (2002) 3053.

[43] F. Millange, C. Serre, J. Marrot, N. Gardant, F. Pelle, G. Férey, J. Mater. Chem. 14 (2004) 642.

[44] J. Jia, X. Lin, A. J. Blake, N. R. Champness, P. Hubberstey, L. Shao, G. Walker, C. Wilson, M. Schroder, Inorg. Chem. 45 (2006) 8838.

[45] H-L. Jiang, N. Tsumori, Q. Xu, Inorg. Chem. 49 (2010) 10001.

[46] X. Guo, G. Zhu, Z. Li, F. Sun, Z. Yang, S. Qiu, Chem. Commun. (2006) 3172.

[47] J. Zhao, L-S. Long, R-B Huang, L-S Zheng, Dalton Trans. (2008) 4714.

[48] J. Xu, J. Cheng, W. Su, M. Hong, Cryst. Growth Des. 11 (2011) 2294.

[49] A. Dimos, D. Tsaousis, A. Michaelides, S. Skoulika, S. Golhen, L. Ouahab, C. Didierjean, A. Aubry, Chem. Mater. 14 (2002) 2616

[50] P. Silva, A. A. Valente, J. Rocha, F. A. A. Paz, Cryst. Growth Des. 10 (2010) 2025.

[51] Q. Yue, J. Yang, G-H. Li, G-D. Li, J-S. Chen, Inorg. Chem. 45 (2006) 4431.

[52] R. F. D'Vries, M. Iglesias, N. Snejko, E. Gutiérrez-Puebla, M. A. Monge, Inorg. Chem. 51 (2012) 11349.

[53] S. Ganguly, P. Pachfule, S. Bala, A. Goswami, S. Bhattacharya, R. Mondal, Inorg. Chem. 52 (2013) 3588.

[54] J. Luo, H. Xu, Y. Liu, Y. Zhao, L. L. Daemen, C. Brown, T. V. Timofeeva, S. Ma, H-C. Zhou, J. Am. Chem. Soc. 130 (2008) 9626.

[55] D-X. Xue, A. J. Cairns, Y. Belmabkhout, L. Wojtas, Y. Liu, M. H. Alkordi, M. Eddaoudi , J. Am. Chem. Soc. 135 (2013) 7660.

[56] J-R. Li, R. J. Kuppler, H-C. Zhou, Chem. Soc. Rev. 38 (2009) 1477.

[57] L. Pan, K. M. Adams, H. E. Hernandez, X. Wang, C. Zheng, Y. Hattori, K. Kaneko, J. Am. Chem. Soc. 125 (2003) 3062.

[58] T. K. Maji, G. Mostafa, H-C. Changa, S. Kitagawa, Chem. Commun. (2005) 2436.

[59] K. L. Gurunatha, S. Mohapatra, P. A. Suchetan, T. K. Maji, Cryst. Growth. Des. 9 (2009) 3844.

[60] J. Duan, M. Higuchi, M. L. Foo, S. Horike, K. P. Rao, S. Kitagawa, Inorg. Chem. 52 (2013) 8244

[61] V. R. Choudhary, S. Mayadevi, Zeolites. 17 (1996) 501.

[62] J. X Zhou, Y. C Zhang, X. W. Guo, A. F. Zhang, X. M. Fei, Ind. Eng. Chem. Res. 45 (2006) 6236.

[63] J. X Zhou, Y. C Zhang. X. W Guo,. W. J. Song, H. L. Bai, A. F Zhang, Energy Fuels 20 (2006) 778.

[64] R. E. Whan, G. A. Crosby, J. Mol. Spectrosc., 8 (1962) 315.

[65] G. A. Crosby, R. E. Whan, R. M. Alire, J. Chem. Phys. 34 (1961) 743.

[66] G. A. Crosby, R. E. Whan, J. J. Freeman, J. Phys. Chem. 66 (1962) 2493.

[67] C. Marchal, Y. Filinchuk, D. Imbert, J.-C.G. Bunzli, M. Mazzanti, Inorg. Chem. 46 (2007) 6242.

[68] X. Guo, G. Zhu, F. Sun, Z. Li, X. Zhao, X. Li. H. Wang,. S. Qiu, Inorg. Chem. 45 (2006) 2581.

[69] X.-P Yang, R. A. Jones, J. H. Rivers, R. Pen-jen Lai, Dalton Trans. (2007) 3936.

[70] S. Ma, X.-S. Wang, D. Yuan, H.-C. Zhou, Angew. Chem., Int. Ed. 47 (2008) 4130.

[71] Q. Yue, J. Yang, G. H. Li, G. D. Li, J. S. Chen, Inorg. Chem. 45 (2006) 4431

[72] B. Yotnoi, A. Rujiwatra, M. L. P. Reddy, D. Sarma, S. Natarajan, Cryst. Growth. Des. 11 (2011) 1347.

[73] S. Ma, D. Yuan, X.-S. Wang, H.-C. Zhou, Inorg. Chem. 48 (2009) 2072.

[74] H.-L. Jiang, N.Tsumori, Q. Xu, Inorg. Chem. 49 (2010) 10001.

[75] J. Luo, H. Xu, Y. Liu, Y. Zhao, L. L. Daemen, C. Brown, T. V Timofeeva,. S. Ma, H.-C. Zhou, J. Am. Chem. Soc. 130 (2008) 9626.

[76] F. S. Richardson, Chem. Rev. 82 (1982) 541.

[77] M. V. Lucky, S. Sivakumar, M. L. P. Reddy, A. K. Paul, S. Natarajan, Crystal Growth & Design. 11 (2011) 857.

[78] P. Mahata, K. V. Ramya, S. Natarajan, Inorg. Chem. 48 (2009) 4942.5

[79] P. Wang, J-P. Ma, Y-B. Dong, R-Q Huang, J. Am. Chem. Soc. 129 (2007) 10620.

[80] H. Guo , Y. Zhu , S. Qiu , J. A. Lercher, H. Zhang, Adv.Mater. 22, (2010) 4190.

[81] K. Liu , Y. Zheng, G. Jia, M. Yang , Y. Song , N. Guo , H. You, J. Solid State Chem. 183 (2010) 2309.

[82] A. R. Ramya, D. Sharma, S. Natarajan, M. L. P. Reddy, Inorg. Chem. 51 (2012) 8818.

[83] X. Zhang, M. A. Ballem, Z.-J. Hu, P. Bergman, K. Uvdal, Angew. Chem. Int. Ed. 50 (2011) 5729.

[84] Y. Luo, G. Calvez, S. Freslon, K. Bernot, C. Daiguebonne, O. Guillou, Eur. J. Inorg. Chem. (2011) 3705.

[85] S. Mohapatra, S. Adhikari, H. Riju, T. K. Maji, Inorg. Chem. 51 (2012) 4891

[86] W. Liu, T. Jiao, Y. Li, Q. Liu, M. Tan, H. Wang, L. Wang, J. Am. Chem. Soc. 126 (2004) 2280.

[87] B. Zhao, X.-Y. Chen, P. Cheng, D.-Z. Liao, S.-P. Yan, Z.-H. Jiang, J. Am. Chem. Soc. 126 (2004) 15394.

[88] B. Chen, L. Wang, Y. Xiao, F. R. Fronczek, M. Xue, Y. Cui, G. Qian, Angew. Chem. Int. Ed. 48 (2009) 500.

[89] A. Bianchi, K. Bowman-James, E. Garcia-Espana, Supramolecular Chemistry of Anions Wiley-VCH: New York, (1997)

[90] P. D. Beer, P. A. Gale, Angew. Chem. Int. Ed. Engl. 40 (2001) 486.

[91] D. Curiel, A. Cowley, P. D. Beer, Chem. Commun. (2005) 236.

[92] R. K. Mahajan, I. Kaur, R. Kaur, S. Uchida, A. Onimarn, S. Shinoda, H. Taukube, Chem. Commun. (2003) 2238.

[93] A. M. Kłonkowski, S. Lis, M. Pietraszkiewicz, Z. Hnatejko, K. Czarnobaj M. Elbanowsk, Chem. Mater. 15 (2003) 656.

[94] K.-L. Wong, G-L. Law, Y.-Y. Yang, W.-T. Wong, Adv. Mater. 18 (2006) 1051.

[95] B. Chen, L. Wang, F. Zapata, G. Qian, E. B. Lobkovsky, J. Am. Chem. Soc. 130 (2008) 6718.

[96] B. Chen, Y. Yang, F. Zapata, G. Lin, G. Qian, E. B. Lobkovsky, Adv. Mater. 19 (2007) 1693.

[97] D. Ma, W. Wang, Y. Li, J. Li, C. Daiguebonne, G. Calvezc, O. Guillou, Cryst. Eng. Comm. 12 (2010) 4372.

[98] B. V. Harbuzaru, A. Corma, F. Rey, P. Atienzar, J. L. Jord, H. Garcia, D. Ananias, L. D. Carlos, J. Rocha, Angew. Chem. Int. Ed. 47 (2008) 1080.

[99] S. V. Eliseeva, D. N. Pleshkov, K. A. Lyssenko, L. S. Lepnev, J.-C.G. Bunzli, N. P. Kuzmina, Inorg. Chem. 49 (2010) 9300.

[100] Y.-W. Lin, B.-R. Jian, S.-C. Huang, C-H. Huang, K.-F. Hsu, Inorg. Chem. 49 (2010) 2316.

[101] H-L. Jiang, Y. Tatsu, Z-H. Lu, Q. Xu, J. Am. Chem. Soc. 132 (2010) 5586.

[102] H. Xu, F. Liu, Y. Cui, B. Chen, G. Qian, Chem. Commun. 47 (2011) 3153.

[103] Y. K. Park, S. B. Choi, H. Kim, K. Kim, B.-H. Won, K. Choi, J.-S. Choi, W-S. Ahn, N. Won, S. Kim, D. H. Jung, S-H. Choi, G-H. Kim, S.-S. Cha, Y. H. Jhon, J. Kuk Yang, J. Kim, Angew. Chem. Int. Ed. 46 (2007) 8230.

[104] R. Sessoli, A. K. Powell, Coord. Chem. Rev. 253 (2009) 2328.

[105] A. Caneschi, D.Gatteschi, R. Sessoli, A. L. Barra, L. C. Brunel, M. Guillot, J. Am. Chem. Soc. 113 (1991) 5873.

[106] R. Sessoli, D. Gatteschi, A. Caneschi, M. A. Novak, Nature 365 (1993) 141.

[107] T. Lis, Acta Crystallogr. Sect. B: Struct. Crystallogr. Cryst. Chem. 36 (1980) 2042.

[108] D. Gatteschi, A. L. Barra, A. Caneschi, A. Cornia, R. Sessoli, L. Sorace, Coord. Chem. Rev. 250 (2006) 1514.

[109] T. N. Nguyen, W. Wernsdorfer, K. A. Abboud, G. Christou, *J. Am. Chem. Soc*. 133 (**2011)** 20688.

[110] A. J. Tasiopoulos, A. Vinslava, W. Wernsdorfer, K. A. Abboud, G. Christou, Angew. Chem. Int. Ed. 43 (2004) 2117.

[111] P.-H. Lin, T. J. Burchell, R. Cl´erac, M. Murugesu, Angew. Chem. Int. Ed. 47 (2008) 8848.

[112] A. M. Ako, I. J. Hewitt, V. Mereacre, R. Cl´erac, W. Wernsdorfer, C. E. Anson, A. K. Powell, Angew. Chem. Int. Ed. 45 (2006) 4926.

[113] K. C. Mondal, A. Sundt, Y. Lan, G. E. Kostakis, O. Waldmann, L. Ungur, L. F. Chibotaru, C. E. Anson, A. K. Powell, Angew. Chem. Int. Ed. 124 (2012) 7668.

[114] A. Caneschi, D. Gatteschi, N. Lalioti, C. Sangregorio, R. Sessoli, G. Venturi, A. Vindigni, A. Rettori, M. G. Pini, M. A. Novak, Angew. Chem. Int. Ed. 40, (2001) 1760.

[115] R. Clérac, H. Miyasaka, M. Yamashita, C. Coulon, J. Am. Chem. Soc. 124 (2002) 12837.

[116] L. Bogani, W. Wernsdorfer, Nat. Mater. 7 (2008) 179.

[117] S. C. Manna, E. Zangrando, A. Bencini, C. Benelli, N. R. Chaudhuri, Inorg. Chem. 45 (2006) 9114.

[118] H.-J. Zhang, X.-Z. Wang, D.-R. Zhu, Y. Song, Y. Xu, H. Xu, X. Shen, T. Gao, M.-X. Huang, Cryst. Eng. Comm 13 (2011) 2586.

[119] Y.-L. Hou, G. Xiong, P.–F. Shi, R.-R. Cheng, J.-Z. Cui, B. Zhao, Chem. Commun. 49 (2013) 606.

[120] W.-H. Fang, L. Cheng, L. Huang, G.-Y. Yang, Inorg. Chem. 52 (2013) 6.

[121] X. Feng, J. Zhao, B. Liu, L. Wang, S. Ng, G. Zhang, J. Wang, X. Shi, Y. Liu, Cryst. Growth Des. 10 (2010) 1399.

[122] A. Datcu, N. Roques, V. Jubera, D. Maspoch, X. Fontrodona, K. Wurst, I. Imaz, G. Mouchaham, J.-P. Sutter, C. Rovira, J. Veciana, Chem. Eur. J. 18 (2012) 152.

[123] Z. Chen, B. Zhao, P. Cheng, X.-Q. Zhao, W. Shi, Y. Song, Inorg. Chem. 48 (2009) 3493.

[124] W. Huang, D. Y. Wu, P. Zhou, W. B. Yan, D. Guo, C. Y. Duan, Q. J. Meng, Cryst. Growth Des. 9, (2009) 1361.

[125] Z.-Y. Li, J.-W. Dai, N. Wang, H.-H. Qiu, S.-T. Yue, Y.-L. Liu, Cryst. Growth Des. 10 (2010) 2746.

[126] B. Zhao, H.-L. Gao, X.-Y. Chen, P. Cheng, W. Shi, D.-Z. Liao, S.-P. Yan, Z.-H. Jiang, Chem.Eur. J. 12 (2006) 149.

[127] D. Maspoch, D. Ruiz-Molina, K. Domingo, M. Cavallini, F. Biscarini, J. Tejada, C. Rovira, J. Veciana, Nat. Mater. 2 (2003) 190.

[128] A. Hazra, P. Kanoo, T. K. Maji, Chem. Commun. 47 (2011) 538.

[129] S. Mohapatra, B. Rajeswaran, A. Chakraborty, A. Sundaresan, T. K. Maji, Chem. Mater. 25 (2013) 1673.

Graphical Abstract:

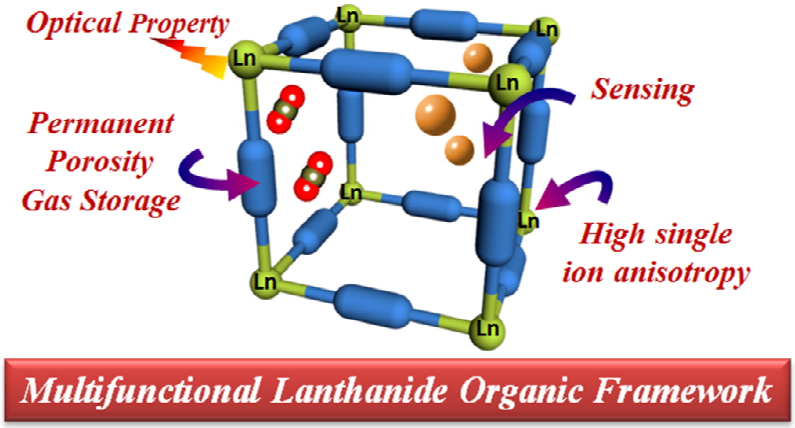

The versatile properties and future promises of multifunctional lanthanide-organic frameworks have been discussed with emphasis on porous, luminescence and magnetic properties.

Highlights

- We present the design strategies of permanently porous Lanthanide-organic frameworks fabrication.
- We discuss the porous and gas adsorption properties of these materials.
- We discuss luminescent frameworks and its application in sensing, colour tunability and white-light emission.
- The single ion anisotropy of such systems are also being discussed which eventually will ensue the slow relaxation of magnetization
- The different magnetic interactions and bi-functional magneto-luminescence in lanthanide-organic frameworks have been discussed.
- We also put forward the future scope of these promising magneto-luminescent lanthanide materials.